



141  
215  
THS

**LIBRARY**  
**Michigan State**  
**University**

This is to certify that the  
thesis entitled

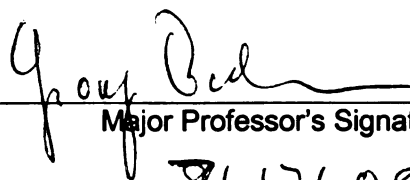
**ACCEPTANCE CALCULATIONS FOR A CHARGE BREEDER  
BASED ON AN ELECTRON BEAM ION TRAP**

presented by

**EMANUEL GAVARTIN**

has been accepted towards fulfillment  
of the requirements for the

M.S. degree in Physics



Major Professor's Signature

7/17/08

Date

**PLACE IN RETURN BOX** to remove this checkout from your record.  
**TO AVOID FINES** return on or before date due.  
**MAY BE RECALLED** with earlier due date if requested.

DATE DUE	DATE DUE	DATE DUE

ACCEPTANCE CALCULATIONS FOR A CHARGE BREEDER BASED  
ON AN ELECTRON BEAM ION TRAP

By

Emanuel Gavartin

A THESIS

Submitted to  
Michigan State University  
in partial fulfillment of the requirements  
for the degree of

MASTER OF SCIENCE

Department of Physics

2008

# **Abstract**

## **ACCEPTANCE CALCULATIONS FOR A CHARGE BREEDER BASED ON AN ELECTRON BEAM ION TRAP**

By

Emanuel Gavartin

The capture of ions in an Electron Beam Ion Trap has been modelled by calculating single ion trajectories and using Monte Carlo techniques to simulate the charge state evolution. By systematically changing the initial conditions of the ion, acceptance of the Electron Beam Ion Trap as a function of the emittance of the injected ion beam has been determined. Different Electron Beam Ion Trap configurations have been studied with the goal to find systems offering both high acceptance and short breeding times into the highest charge states. The results will be used in the design of an Electron Beam Ion Trap charge breeder which will be the first stage of a reaccelerator for rare isotope beams presently under construction at the National Superconducting Cyclotron Laboratory (NSCL).

# ACKNOWLEDGMENTS

I am deeply indebted to my adviser, Prof. Georg Bollen, for guiding my research through strong academic support and giving me the opportunity to contribute to the development of the NSCL charge breeder. I wish to thank Dr. Stefan Schwarz. Without his guidance, patience and encouragement this thesis could hardly have been realized.

I gratefully acknowledge the support of the Studienstiftung des deutschen Volkes for giving me orientation during the entire period of my studies, and for the financial support during my stay at MSU.

I would like to thank Brad Barquest for many fruitful discussions and proof-reading this thesis. Special thanks are due to my family and my friends Tobias Hahn and Sarah Heim for giving me encouragement during my time at MSU.

# Contents

<b>List of Tables</b> . . . . .	<b>vi</b>
<b>List of Figures</b> . . . . .	<b>vii</b>
<b>1 Introduction</b> . . . . .	<b>1</b>
1.1 ECR-based charge breeding . . . . .	2
1.2 EBIT-based charge breeding . . . . .	3
1.3 Goal of the thesis . . . . .	5
<b>2 Physics of Electron beam ion traps and sources</b> . . . . .	<b>6</b>
2.1 Electron beam . . . . .	7
2.2 Motion of an ion in an EBIT . . . . .	9
2.3 Charge evolution . . . . .	11
2.4 Ion injection and capture . . . . .	13
2.5 Extraction of ions . . . . .	14
2.6 Emittance and Acceptance . . . . .	15
<b>3 Development of an Electron Beam Ion Trap charge breeder</b> . . . . .	<b>17</b>
3.1 NSCL reaccelerator concept . . . . .	17
3.2 Status of the charge breeder at the NSCL . . . . .	18
3.2.1 Electron gun . . . . .	18
3.2.2 Trap . . . . .	20
3.2.3 Collector . . . . .	21
<b>4 Development of an EBIT simulation code</b> . . . . .	<b>22</b>
4.1 Simulation algorithm for ion dynamics . . . . .	23
4.2 Trap setup . . . . .	23
4.3 Ionization . . . . .	25
4.4 Capture of ions . . . . .	26
4.5 Injection of ions . . . . .	26
4.6 Evaluation of axial potential . . . . .	27
4.7 Electron beam energy . . . . .	28
4.8 Other simulation parameters . . . . .	28
4.9 Code test by energy conservation . . . . .	29
<b>5 Acceptance calculations</b> . . . . .	<b>31</b>
5.1 Determining the capture probability . . . . .	31
5.2 Acceptance . . . . .	32
5.3 Capture probability . . . . .	33

<b>6</b>	<b>Investigation of different field configurations for the NSCL charge breeder .</b>	<b>37</b>
6.1	Magnetic field . . . . .	37
6.2	Potential configuration and electron beam energy in the trap . . . . .	41
6.3	Electron beam current . . . . .	44
<b>7</b>	<b>Results . . . . .</b>	<b>46</b>
7.1	Charge evolution of an injected ion . . . . .	46
7.2	Magnetic field . . . . .	47
7.2.1	Capture probability . . . . .	47
7.2.2	Position at first ionization . . . . .	48
7.2.3	Magnetic field at first ionization . . . . .	50
7.2.4	Charge state after successful capture . . . . .	51
7.2.5	Comparison between the ‘1T-6T’ and the ‘6T-1T’ configuration . .	51
7.3	Electron beam energy . . . . .	54
7.4	Electron beam current . . . . .	57
7.5	Trap dimensions . . . . .	58
7.6	Initial axial energy . . . . .	59
<b>8</b>	<b>Summary and conclusions . . . . .</b>	<b>62</b>
	<b>APPENDICES . . . . .</b>	<b>65</b>
<b>A</b>	<b>Function for the ionization process . . . . .</b>	<b>65</b>
	<b>Bibliography . . . . .</b>	<b>71</b>

## List of Tables

4.1	Common parameters used in the simulation. . . . .	29
6.1	Dimensions of the coil configuration, and the pre-factors from Equation 4.2 for the different magnetic field configurations . . . . .	41
7.1	Percentage of ions that are ionized before ('Before') and after ('After') the reflection at the second barrier. . . . .	50
7.2	Percentages for capture and various loss mechanisms. <i>Trapped</i> refers to the case, when an ion is considered captured. <i>Wall</i> refers to the case, when an ion is lost by hitting an electrode. <i>Lost</i> refers to the case, when an ion is not trapped after one round-trip. <i>Reflected</i> refers to the case, when an ion is reflected by the first potential barrier. . . . .	55
7.3	Percentage of ions that are ionized before ('Before') and after ('After') the reflection at the second barrier for three electron beam currents with an electron beam energy of $E_e = 12 - 13$ keV. . . . .	58
7.4	Percentage of ions that are ionized before ('Before') and after ('After') the reflection at the second barrier. 'Long' indicates that the trapping region was made 20 cm longer. The electron beam energy is $E_e = 12 - 13$ keV. .	59

## List of Figures

1.1	Charge state evolution for $\text{Ti}^+$ -ions in an EBIT with a current density of $10^4 \text{ A/cm}^2$ and an electron energy of 5 keV. . . . .	4
2.1	Schematic view of an EBIT. . . . .	7
2.2	Radial space charge potential for an electron beam with radius $r_H = 26.4 \mu\text{m}$ , electron energy $E_e = 9.2 \text{ keV}$ , electron current $I_e = 1 \text{ A}$ inside a cylindrical electrode with radius $r_T = 10 \text{ mm}$ . . . . .	9
2.3	Principle of the pulsed injection mode. . . . .	13
2.4	Principle of the continuous injection mode, or accumulation mode. . . . .	14
2.5	The leaky-mode (left) and pulsed extraction (right) scenarios. . . . .	14
2.6	Concept of emittance and acceptance. A set of points representing the emittance of an injected beam is shown on the left and the acceptance of a system is illustrated on the right. The overlap between both areas gives the fraction of the beam that is transported in the system without losses. . . . .	16
3.1	Scheme of the EBIT-based $\text{N}^+$ reacceleration under development at the NSCL [29]. . . . .	18
3.2	Section view of the electron gun assembly. The cathode emits electrons that are accelerated and extracted through the anode. . . . .	19
3.3	Section view of the collector assembly. . . . .	21
4.1	Schematic view of the EBIT setup as used in the code, not to scale. . . . .	24
4.2	Illustration of a finite sized solenoid used to calculate the axial magnetic field. . . . .	25
4.3	Test if code correctly handles electric fields due to applied and space charge potential. The figure shows the analytically calculated potential energy, the kinetic energy from the integration of the equations of motion and the sum. In (a) the ion is injected on-axis with no transverse velocity. In (b) the ion is injected at $r_{in} = 1 \cdot 10^{-3} \text{ m}$ , $v_r = 13851 \text{ m/s}$ and $v_\phi = 0 \text{ m/s}$ . . . . .	30
5.1	Flow chart for the acceptance calculation. . . . .	33

5.2	Example of an acceptance plot calculated for $ x  < 4.75$ mm and $ x'  < 25$ mrad. The configuration used is the '1T-6T'-configuration, described in Section 6.1 . . . . .	34
5.3	Flow chart of the capture probability calculation. . . . .	36
6.1	Comparison between three magnetic field configurations (a). Corresponding electron beam radii as given by the Herrmann radius $r_H$ (b) . . . . .	39
6.2	Axial potential for different magnetic field configurations. Top: Potentials obtained from applying voltages to the electrodes. Bottom: Potentials including space charge effects. . . . .	40
6.3	Potential and axial magnetic field configurations on axis. The different curves show the potential produced by the electrodes (dot-dash), the total potential including space charge effects (dot) and the magnetic field (solid). The electron beam current is $I = 2.5$ A. . . . .	42
6.4	Electron beam energy distribution generated using the potential given by the voltages applied on the electrodes as specified in Figure 6.3. Space charge effects are neglected. . . . .	44
6.5	Axial on-axis potential configurations for '1T-6T' showing potential without space charge and with space charge for different electron currents. . . .	45
7.1	Charge evolution for a Ti-ion. The '1T-6T'-configuration is used with an electron energy of $E_e = 10 - 11$ keV and an electron beam current of $I_e = 2.5$ A. Left: Average ionization time to reach a charge state. Right: Ionization probability to reach a certain charge state within $t_{cut} = 5 \cdot 10^{-4}$ s. 47	47
7.2	Comparison of the capture probability as a function of emittance for three different magnetic field configurations. The calculations were performed for electron beam energies of (a): $E_e = 10 - 11$ keV, (b): $E_e = 12 - 13$ keV and (c): $E_e = 13 - 14$ keV in the trap. The electron current is $I_e = 2.5$ A. .	48
7.3	Histogram for the position of the first ionization after injection for the three configurations (a): '1T-6T', (b): '6T-6T', (c): '6T-1T'. The data is taken are the simulations with an electron beam energy of $E_e = 12 - 13$ keV. The upper half of a histogram shows the ionization for the in-going beam. The lower half shows the percentage of $1^+ \rightarrow 2^+$ ionization after the ions have been turned around at the second barrier. . . . .	49

7.4	Histogram of the probability for an ion to undergo the first ionization at a certain magnetic field. The histograms show the three different cases (a): '1T-6T', (b): '6T-6T', (c): '6T-1T'. The electron beam energy in the trap is $E_e = 12 - 13$ keV. . . . .	52
7.5	Histogram of the charge state of the ion, when it is considered captured. The histograms show the three different cases (a): '1T-6T', (b): '6T-6T', (c): '6T-1T'. The electron beam energy in the trap is $E_e = 12 - 13$ keV. . .	53
7.6	Comparison of the capture probability as a function of emittance for different electron beam energies. Three different configurations are considered with (a): '1T-6T', (b): '6T-6T' and (c): '6T-1T'. The electron current is $I_e = 2.5$ A. . . . .	56
7.7	Comparison of the capture probability as a function of emittance for different electron beam currents for the '1T-6T'-configuration. The electron beam energy inside the trap is $E_e = 12 - 13$ keV. . . . .	57
7.8	Comparison of the capture probability as a function of emittance for different trap lengths. 'Long' indicates that the trapping region was made 20 cm longer. The electron beam current is $I_e = 2.5$ A and the electron beam energy is $E_e = 12 - 13$ keV. . . . .	59
7.9	Comparison of the capture probability as a function of emittance for ions with different initial axial energies. The electron beam energy inside the trap is $E_e = 12 - 13$ keV. . . . .	61

IMAGES IN THIS THESIS ARE PRESENTED IN COLOR.

# Chapter 1

## Introduction

Rare Isotope Beams (RIBs) are created at the NSCL by the in-flight particle fragmentation method [1, 2]. This is a powerful approach to reach isotopes far from the valley of stability without chemical limitations. Very sensitive experiments can be performed, because the fast beams allow single ion identification. However, the high energy in the order of 100 MeV/u of the beams from projectile fragmentation is not always of advantage. Certain experiments in the areas of nuclear astrophysics, nuclear reaction and nuclear structure require beam energies in the range of a few 100 keV/u and up to about 10 MeV/u. Deacceleration of the fast beams or slowing them down in matter is normally not an option, since this causes an unacceptable deterioration of the beam quality. At Isotope Separator on-line (ISOL) facilities like ISOLDE at CERN, ISAC at TRIUMF, or HRIBF at ORNL, beams in this energy range are generated by reaccelerating the low-energy beams (60 keV/u) available from ISOL beam production.

At the NSCL a project is under way that will allow reacceleration of rare isotopes for projectile fragmentation. The key to this is a technique called gas stopping, where the fast beams are slowed down in matter and finally stopped in pure helium. Singly charged ions are extracted from the stopping cell and a low-energy beam is formed. These thermalized rare isotope beams have already been successfully used at the NSCL for a series of high-

precision mass measurements with a Penning trap mass spectrometer [3–5].

In the first phase of the NSCL reaccelerator project it is foreseen to accelerate the rare isotope beams to 0.3-3 MeV/u. For optimum performance the reaccelerator should most importantly operate with high efficiency for ions of all elements that are available at the NSCL, and provide a high beam purity to avoid ambiguities resulting from background ions [6]. In order to achieve such a performance the NSCL has opted for an acceleration scheme that involves charge breeding with an Electron Beam Ion Trap.

The classical and well-established approach is the acceleration and subsequent stripping of singly charged ions. However, such a  $1^+$  reacceleration scheme is complex and needs large numbers of accelerator modules. As a consequence it is more costly than possible alternatives. Moreover, there is a significant decline in efficiency for heavier ion beams. This loss is exacerbated by the necessity of multiple charge-state strippers [7].

To improve the reacceleration performance a charge breeder can be implemented as a first step in a reaccelerator. This allows a very compact and cost-efficient scheme. In order for the efficiency of the  $N^+$  scheme to surpasses that of the  $1^+$  scheme, a high efficiency has to be obtained to breed ions into a single high charge state.

## **1.1 ECR-based charge breeding**

The most common approach to generate highly charged ions is to use Electron Cyclotron Resonance Ion Sources (ECRIS). In an ECRIS ions of the desired element are held in a volume by a magnetic field. This magnetic field defines the cyclotron frequency of the ions. Microwaves of this frequency are guided into the source in order to heat free electrons present in the source volume. Ionization of the ions is caused through collision of the accelerated free electrons with the ions.

There is a lot of experience with ECRIS, since they are used as sources of high intensity and highly charged ions for stable beam acceleration. Thus they are also considered as

possible charge breeders [8]. Several studies have been performed with these systems, and the PHOENIX source [9] is one example of a charge breeder system based on ECRIS. Tests with stable beams revealed a breeding efficiency of about 4% for  $\text{Sn}^{1+} \rightarrow \text{Sn}^{22+}$ . Typical breeding times for such charge states are around 100 ms. Disadvantages of ECRIS systems are broad charge state distributions, long breeding times, and the presence of large currents ( $> \text{mA}$ ) of stable ions that give an undesired background.

## 1.2 EBIT-based charge breeding

An alternative to ECRIS systems for the charge breeding of ions are Electron Beam Ion Sources or Traps (EBIS/Ts). EBIS/Ts use a magnetically compressed electron beam to radially trap and charge breed ions. An electrostatic field, produced by a number of trap electrodes, provides axial confinement. After the charge breeding process the ions can be extracted using various techniques described later. While EBIT devices have been mainly used for spectroscopic studies of trapped, highly-charged stable ions, EBISs have been used as sources of highly charged ion beams. Reacceleration with charge breeding based on an EBIS was first demonstrated at REX-ISOLDE [10] at CERN with REX-EBIS [11] used as a charge breeder. It operates with an electron current of 200-250 mA, allowing the breeding of  $\text{Na}^{1+}$  to  $\text{Na}^{8+}$  (peak charge) within 18 ms. Breeding times of 150 ms have been found for the  $\text{Cs}^{1+}$  to  $\text{Cs}^{32+}$  charge breeding process. Average charge breeding efficiencies of 10%, and in some cases  $>20\%$  have been observed [11]. Brookhaven National Lab has successfully developed a high performance Electron Beam Ion Source, the RHIC Test EBIS [12], for stable beams. Such a system will be used for providing intense pulses of highly charged ions for RHIC.

Marrs and Slaughter analyzed the possibility to use a high-intensity EBIT (5 A,  $10^5 \text{ A/cm}^2$  for 30 keV electrons) as a charge-booster for the Rare Isotope Accelerator project [13]. Their findings indicate that an EBIT would have charge breeding properties

for rare isotopes superior to any other device at present. Particularly narrow charge state distributions can be obtained by changing the electron beam energy. Breeding efficiencies of up to 90% can be achieved for closed shell configurations [14]. Closed-shell breeding is demonstrated in Figure 1.1 which shows the calculated charge state evolution for  $\text{Ti}^{+}$ -ions in an EBIT [6]. For the electron energy of 5 keV used in the simulations the breeding process stops at the He-like configuration after a breeding time of about 10 ms, because the electron beam energy used is lower than the ionization potential of the next electron to be removed.

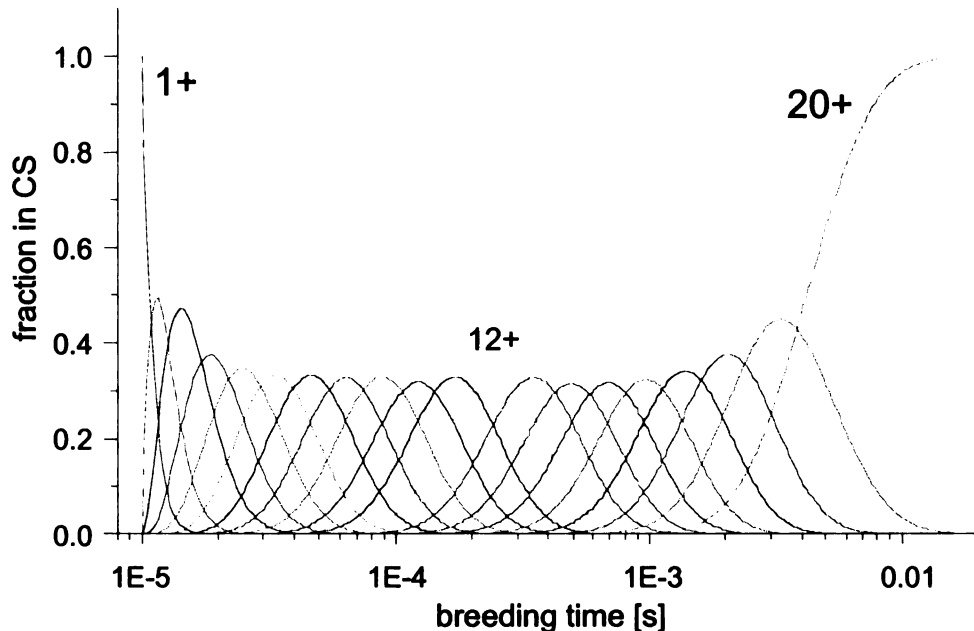


Figure 1.1. Charge state evolution for  $\text{Ti}^{+}$ -ions in an EBIT with a current density of  $10^4 \text{ A/cm}^2$  and an electron energy of 5 keV.

Recently an EBIT charge breeder was built at the Max Planck Institute for Nuclear Physics in Heidelberg as part of a collaboration with TRIUMF [15]. This charge breeder will be used for TITAN [16], which is an ion trap project dedicated to high-precision mass measurements of highly charged ions of rare isotopes produced at ISAC. The device is now being commissioned at TRIUMF. Since the expected performance of this charge breeder is close to the requirements for an efficient reacceleration scheme, the NSCL-EBIT will be

similar to the TITAN charge breeder.

### **1.3 Goal of the thesis**

The goal of this thesis has been the development of a simulation code for the determination of the acceptance of the EBIT, i.e., the probability for an ion beam to be captured as a function of its emittance. The simulation code is based on calculating trajectories of the injected ions and simulating the ionization processes in the trap by using Monte Carlo techniques. The code has been used to study various scenarios that include different magnetic field configurations, electrode systems and injection parameters for the NSCL-EBIT.

## **Chapter 2**

# **Physics of Electron beam ion traps and sources**

EBIS/Ts are devices that allow the creation of highly charged ions [17]. An EBIS/T uses a high current electron beam that is magnetically compressed to trap and sequentially ionize ions to a high charge state. Figure 2.1 schematically shows the setup of an EBIS/T. The major components of the EBIS/T are the electron gun, the trap and the collector. The electron gun produces a high current electron beam that is accelerated into the trap region. The trap region consists of several near-cylindrically shaped electrodes to provide an axial trapping potential and is surrounded by magnetic coils providing a strong magnetic field. The electron beam is compressed by the increasing magnetic field. After passing the trap region, the electron beam expands due to the decreasing magnetic field and is collected on the inner face of the collector. The ions are injected through the collector into the EBIT.

E. D. Donets invented the electron beam ion source (EBIS) [18]. Following related work by Schmieder [19], the first electron beam ion trap (EBIT) was developed by Levine [20]. EBITs typically have a split coil arrangement allowing the installation of radial observation ports [17]. They are often used for atomic spectroscopy, and are generally constructed with a shorter trapping region than an EBIS.

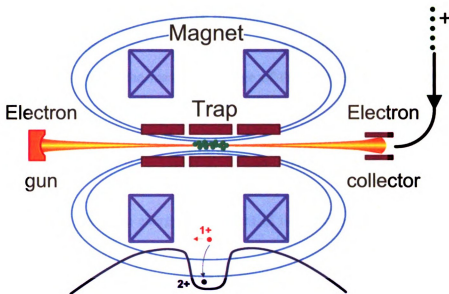


Figure 2.1. Schematic view of an EBIT.

In the literature there is often a distinction made between EBISs and EBITs. The primary purpose of an EBISs is to deliver highly charged ions to other experiments while EBITs refrain the charge bred trapped ions for *in situ* studies. However, the distinction is somewhat arbitrary as EBITs are now becoming sources of highly charged ions.

Since the NSCL charge breeder will have radial observation ports requiring a split coil configuration, it will be labelled an EBIT for subsequent discussion.

## 2.1 Electron beam

The radial dimensions of the electron beam travelling through an EBIT can be described by the Herrmann radius [21], which gives a good prediction for the radius  $r_H$  through which 80% of the beam passes as

$$r_H = r_b \sqrt{\frac{1}{2} + \frac{1}{2} \sqrt{1 + 4 \left( \frac{8 m_e k T r_c^2}{e^2 r_b^4 B^2} + \frac{B_c^2 r_c^4}{B^2 r_b^4} \right)}}, \quad (2.1)$$

where  $r_c$  is the cathode radius in the electron gun,  $T$  is the cathode temperature,  $k$  is Boltzmann's constant,  $B_c$  is the magnetic field at the cathode,  $B$  is the magnetic field strength and  $m_e$  and  $e$  are the mass and charge of the electron, respectively.  $r_b$  is the Brillouin radius [22] given by

$$r_b = \frac{1}{B} \sqrt{\frac{I_e}{\pi \epsilon_0}} \left( \frac{2m_e^3}{E_e e^2} \right)^{1/4}, \quad (2.2)$$

with  $E_e$  and  $I_e$  being the energy and current of the electron beam, and  $\epsilon_0$  being the vacuum permittivity.

The space charge of the electron beam leads to an electrostatic potential. It was discussed [23] that a Gaussian distribution is a good approximation for an electron beam profile. For such a case it is possible to calculate the potential in a closed form, however the expression is rather complicated and not well suited for numerical studies. It was noted [24] that a distribution assuming a uniform charge density of the electron beam up to a fixed radius, and a vanishing density beyond this radius, also offers good results when compared to measurements. This so called top-hat profile allows straightforward calculations of the equations of motion, and is used for the simulations performed in this work. The radius up to which a uniform charge distribution is assumed is taken equal to the Herrmann radius. The electric potential  $\phi$  as a function of radius  $r$  is then given by

$$\phi = \frac{Q_e}{2\pi\epsilon_0} \begin{cases} \left[ \frac{1}{2} \left( 1 - r^2/r_H^2 \right) + \ln(r_T/r_H) \right] & : 0 \leq r < r_H \\ \ln(r_T/r) & : r_H \leq r < r_T, \end{cases} \quad (2.3)$$

with the linear charge density  $Q_e < 0$  and the radius of the cylindrical electrode  $r_T$  through which the electron beam is assumed to pass.  $Q_e$  is given by  $I_e/v_e$ ,  $v_e$  being the velocity of the electrons in the beam.

As an example Figure 2.2 shows the radial space charge potential for the conditions  $r_H = 26.4 \mu\text{m}$ ,  $E_e = 9.2 \text{ keV}$ ,  $I_e = 1 \text{ A}$ ,  $r_T = 10 \text{ mm}$ . The space charge provides a

substantial radial trapping potential for the ions as can be seen from Figure 2.2.

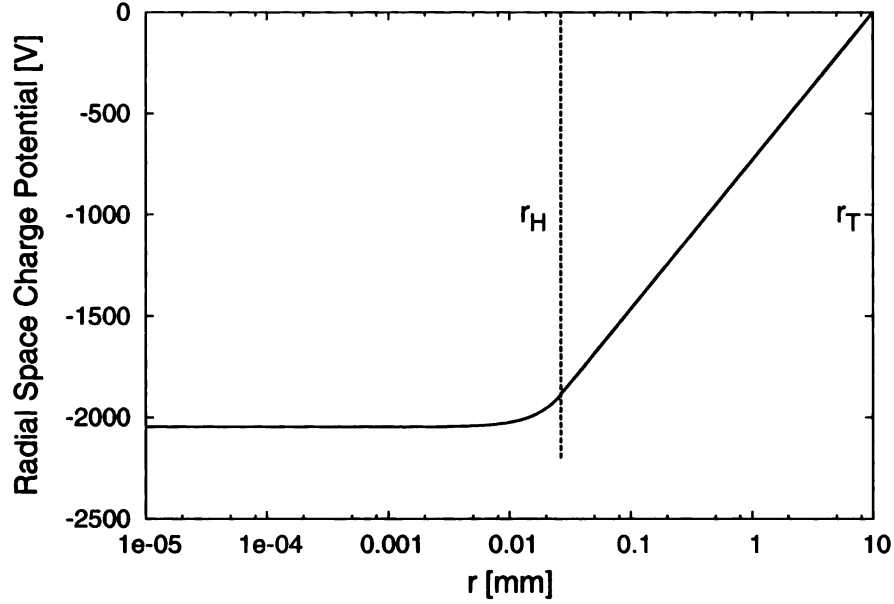


Figure 2.2. Radial space charge potential for an electron beam with radius  $r_H = 26.4 \mu\text{m}$ , electron energy  $E_e = 9.2 \text{ keV}$ , electron current  $I_e = 1 \text{ A}$  inside a cylindrical electrode with radius  $r_T = 10 \text{ mm}$ .

## 2.2 Motion of an ion in an EBIT

Due to the axial symmetry of the device it is convenient to describe the motion of an ion in an EBIT in cylindrical coordinates. In the radial direction the movement of a trapped ion in an EBIT is determined by the radial electrical field  $E_r$  with

$$E_r = -\nabla_r \phi, \quad (2.4)$$

and by the Lorentz force resulting from the axial magnetic field component  $B$ . Thus we arrive at equations of motion in the transverse coordinates  $x$  and  $y$

$$\ddot{x} = \frac{q}{m} \frac{Q_e}{2\pi\epsilon_0} \frac{1}{r_H^2} x + \frac{q}{m} B \dot{y} \quad (2.5)$$

$$\ddot{y} = \frac{q}{m} \frac{Q_e}{2\pi\epsilon_0} \frac{1}{r_H^2} y - \frac{q}{m} B \dot{x} \quad (2.6)$$

for  $r \leq r_H$  and

$$\ddot{x} = \frac{q}{m} \frac{Q_e}{2\pi\epsilon_0} \frac{1}{x^2 + y^2} x + \frac{q}{m} B \dot{y} \quad (2.7)$$

$$\ddot{y} = \frac{q}{m} \frac{Q_e}{2\pi\epsilon_0} \frac{1}{x^2 + y^2} y - \frac{q}{m} B \dot{x}, \quad (2.8)$$

for  $r_H < r \leq r_T$ , with  $q$  and  $m$  being the charge and mass of the ion, respectively.

Comparing the contributions resulting from the electron beam and the Lorentz force, we can estimate which effect is dominant in the equations of motion. The ratio between the two summands in Equation 2.5 is

$$R = \frac{Q_e \cdot x / (2\pi\epsilon_0 r_H^2)}{B \cdot \dot{y}}. \quad (2.9)$$

As an example, let's use typical parameters for a high-intensity EBIT:  $I_e = 2$  A,  $E_e = 5$  keV,  $B = 3$  T,  $r_H = 26.4 \mu\text{m}$ ,  $r_T = 10$  mm. For the average transverse position we take  $x = r_H/2$  and for  $\dot{y}$  we use the velocity the ion has gained at  $y = r_H/2$  when starting at rest at  $y = r_H$ . For these values we obtain  $R \approx 164$ , which shows that the dominant effect in the equations of motion is the space charge of the electron beam.

The axial motion is determined by the electric field  $E_{z,\text{ext}}$  created by voltages applied to the cylindrical electrodes, and by the electric field of the space charge

$$E_{z,\text{el}} = -\frac{\partial\phi}{\partial z}. \quad (2.10)$$

Thus the equation of motion in the  $z$ -direction is

$$\ddot{z} = \frac{q}{m} (E_{z,\text{ext}} + E_{z,\text{el}}) . \quad (2.11)$$

To good approximation for small ion radii the radial magnetic field component is given by

$$B_r = -\frac{1}{2} \frac{\partial B_z}{\partial z} r. \quad (2.12)$$

This should be included in the equations of motion. However, since the radial field component is small under the conditions assumed for the EBIT considered in this work, the radial magnetic field can to good approximation be neglected in the calculations.

Axial trapping is obtained by applying voltages to the series of cylindrical electrodes in the trap. Usually, the central electrode is negatively biased with respect to the outer electrodes, so that the trapped ions cannot escape unless the applied voltages are changed.

If voltages are applied on the electrodes, also radial electric field components are produced besides the axial field. Again, this effect is not considered in the calculations.

## 2.3 Charge evolution

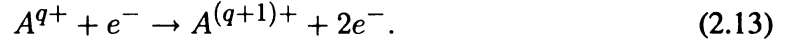
One of the objectives of an EBIT is to produce highly charged ions through interaction with the electron beam. Since probabilities for multiple ionization processes are low, the higher charge-states are mainly obtained by sequential ionization. Processes that can take place in an EBIT operated with current densities of about 40000 A/cm<sup>2</sup> and with their typical time-scales are:

- electron impact ionization of ions ( $< 10 \mu\text{s}$  for  $1^+ \rightarrow 2^+$  process)
- radiative recombination of ions ( $< 10 \mu\text{s}$ )

- charge exchange between ions and neutral atoms or between ions and ions  
(0.1 ms–1 ms)
- ion heating by the electron beam (10 ms–10 s)
- ion-ion energy exchange (0.1 ms–1 ms)

Since processes regarding charge evolution occur on a much smaller time-scale than any others, only these processes are important for the simulation. For low charge states the cross-sections of the electron impact process are much larger than those of radiative recombination and charge exchange processes. Thus only electron impact is described in this section, while details about the other processes can be found in [24].

Electron impact ionization for a charged ion  $A^{q+}$  is described by the following process



The cross-section  $\sigma_{\text{EI}}$  for this process for a certain charge state of a specific ion can be described by W. Lotz's semi-empirical formula [25]

$$\sigma_{\text{EI}}(E_e) = \sum_{j=1}^n a_j q_j \frac{\ln(E_e/I_{p_j})}{E_e I_{p_j}} \left[ 1 - b_j \exp\left(-c_j \left(E_e/I_{p_j} - 1\right)\right) \right], \quad (2.14)$$

$a_j$ ,  $b_j$  and  $c_j$  being parameters that have to be determined for a specific ion,  $I_{p_j}$  being the required ionization energy,  $E_e$  being the energy of the electron beam. It is  $E_e > I_{p_j}$ , and the sum in Equation 2.14 goes over all main shells  $j$  that are totally or partially filled.

The probability for  $1^+ \rightarrow 2^+$  ionization by electron impact as a function of the time  $t_{iEB}$  the ion spends inside the electron beam can be given as

$$p = 1 - \exp(-t_{iEB}/t_{1 \rightarrow 2}), \quad (2.15)$$

with  $t_{1 \rightarrow 2} = e / (\sigma_{\text{EI}} \cdot j_e)$ .  $j_e$  is the current density of the electron beam and is given by

$$j_e = \frac{0.8 \cdot I_e}{\pi r_H^2}. \quad (2.16)$$

The factor 0.8 is a consequence of the definition that the area  $\pi r_H^2$  encloses 80% of the electron beam.

## 2.4 Ion injection and capture

Ions can be injected into an EBIT as a pulsed or a continuous beam. Pulsed beam injection is illustrated in Figure 2.3. During the injection the outer electrode at the electron collector side is at the same voltage as the electrodes in the trap. This way there is no potential barrier and the pulsed ion beam can be injected. After injection the potential of the outer electrode is raised, so that it is higher than the trapping electrode potential thus confining the ions axially. To capture the ions their axial energy has to be lower than the potential of the outer electrodes. At REX-EBIS the pulsed mode is used, and the ion beam is cooled and bunched with a Penning trap before entering the EBIT [26]

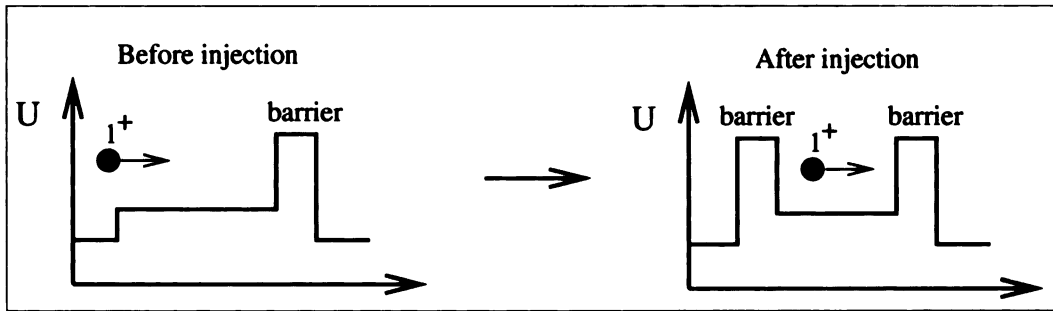


Figure 2.3. Principle of the pulsed injection mode.

For continuous ion beam injection the potential distribution of the outer and trap electrodes does not change with time (see Figure 2.4). In order for the ions to be trapped, they have to undergo at least one ionization step during their round-trip after being injected into

the EBIT. The advantage of this accumulation-mode is the elimination of a buncher before injection.

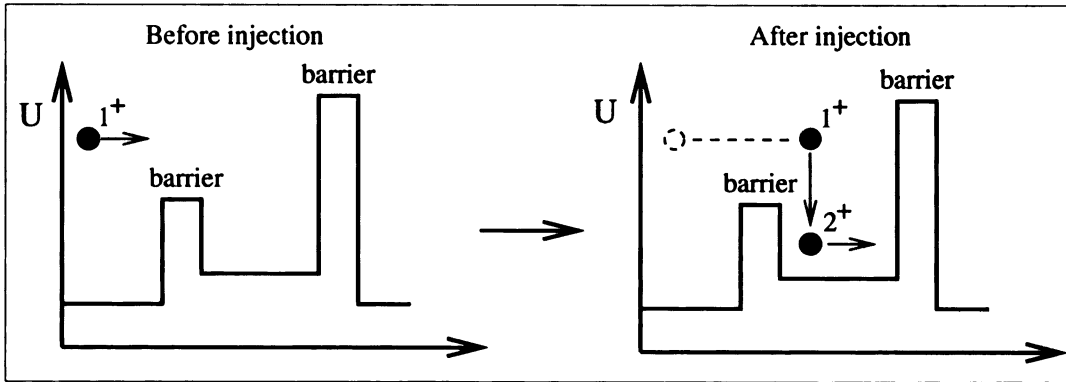


Figure 2.4. Principle of the continuous injection mode, or accumulation mode.

## 2.5 Extraction of ions

The two common scenarios to extract ions from an EBIT are illustrated in Figure 2.5. The simplest to use is the leaky mode, where the height of the potential barriers is different, so that the lowest value of both potentials determines the trap depth. Ions having a larger axial kinetic energy than the lower barrier can escape through continuous evaporation [27].

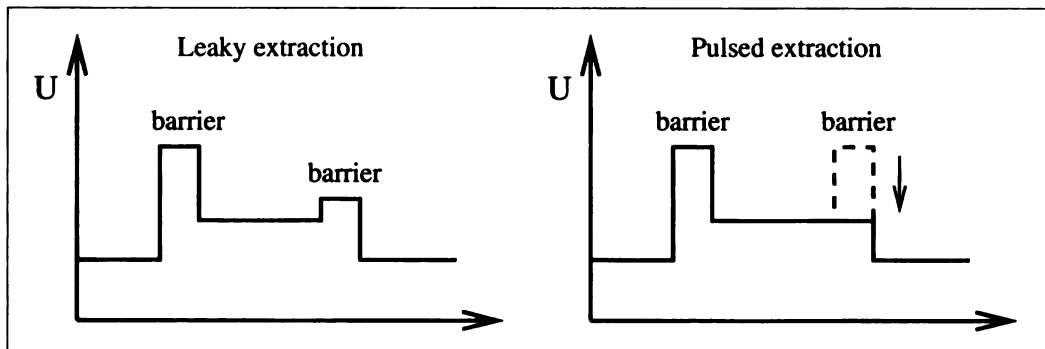


Figure 2.5. The leaky-mode (left) and pulsed extraction (right) scenarios.

Another possibility, called pulsed extraction, is to either raise the potential of the central

trap electrode above that of the outer electrodes or to lower the potential of one of the outer electrodes.

High-charge state ions have lower escape rates in leaky mode operation, because of the higher trap potential for higher ion charge states [27]. For this reason it is preferable to use the pulsed extraction of ions, so that effective extracting is also possible for the highest charge states [17].

## 2.6 Emittance and Acceptance

In order to be able to quantify ion beam properties, the concept of emittance is used. The emittance is defined as the volume occupied by the beam in the six-dimensional phase-space consisting of the position and momentum coordinates of the horizontal, vertical and longitudinal directions. The longitudinal direction corresponds to the propagation direction of the beam. Longitudinal emittance is important for pulsed beams; it will not be discussed here and further details are given in [28]. The horizontal and vertical degrees of freedom constitute the transverse emittances.

Transverse emittance  $\epsilon$  is an indicator of the quality of a continuous beam. Assuming that the beam is propagating along the  $z$ -direction, a phase space plot is a plot of the  $x$ - $x'$  (horizontal) or  $y$ - $y'$  (vertical) values for all particles of the beam at a certain position  $z$ .  $x'$  and  $y'$  are defined as  $x' = v_x/v_z$  and  $y' = v_y/v_z$  [28],  $v_x$  and  $v_y$  being the velocities in the  $x$  and  $y$  directions, respectively.

The ion beam injected into the EBIT has a certain emittance. The EBIT itself has a certain acceptance of the incoming beam, again defined as an area in phase-space. The overlap between the emittance of the incoming ion beam and the acceptance of the EBIT at the injection point gives the fraction of ions that will be captured. Figure 2.6 illustrates this concept.

Due to the axial symmetry of the EBIT the horizontal and vertical acceptances are

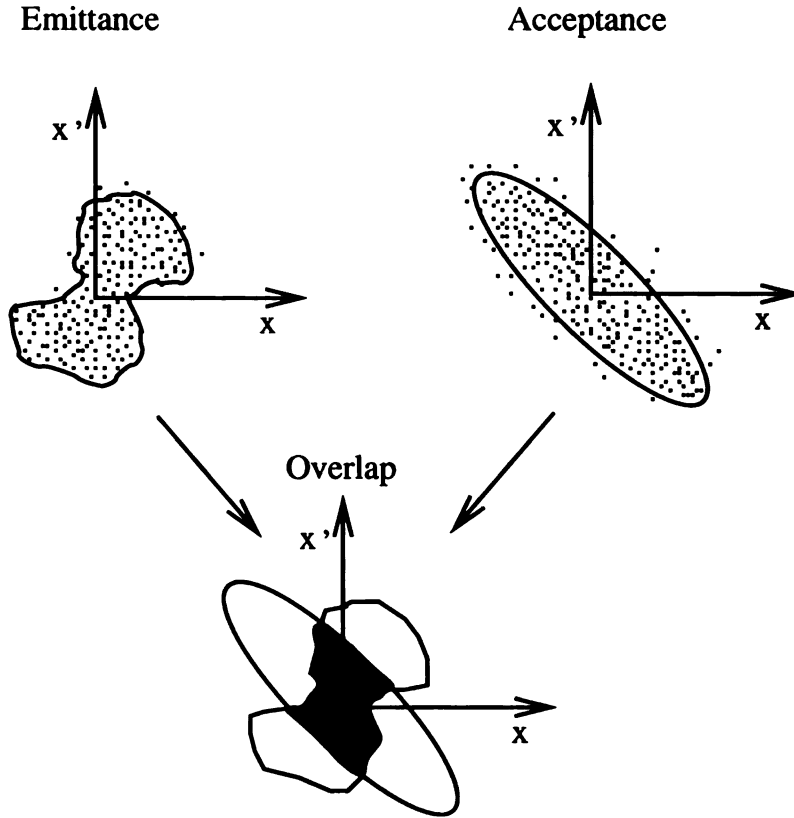


Figure 2.6. Concept of emittance and acceptance. A set of points representing the emittance of an injected beam is shown on the left and the acceptance of a system is illustrated on the right. The overlap between both areas gives the fraction of the beam that is transported in the system without losses.

identical.

Since the definitions of  $x'$  and  $y'$  rely on the magnitude of  $v_z$ , emittances for ion beams injected with different axial energies have to be scaled in order to be comparable. The emittance values are transformed from the emittance  $\epsilon_1$  at the axial energy of the ions  $E_1$  to the emittance  $\epsilon_2$  at another energy  $E_2$  by

$$\epsilon_2 = \epsilon_1 \cdot \sqrt{\frac{E_1}{E_2}}. \quad (2.17)$$

## **Chapter 3**

# **Development of an Electron Beam Ion Trap charge breeder**

### **3.1 NSCL reaccelerator concept**

The NSCL  $n^+$  reaccelerator concept is shown in Figure 3.1. The rare isotope beam (RIB) coming from the fragment separator and after being stopped and thermalized in the gas stopper (not shown) is sent into the EBIT which is located on a high voltage platform. To match the velocity of the highly charged ions to the requirements of the radio-frequency quadrupole (RFQ) accelerator, the platform voltage can be raised to several tens of kV for extraction. An achromatic Q/A separator selects the desired charge state of the extracted ions and suppresses unwanted background ions. The Low Energy Beam Transport system (LEBT) transports ions from the EBIT to the RFQ. The beam is initially accelerated by the RFQ to 600 keV/u. Further acceleration is achieved in a superconducting linac (SC linac) to an energy of up to 3 MeV/nucleon. A High Energy Beam Transport system (HEBT) delivers the RIB to the experimental area. Further details are given in [29].

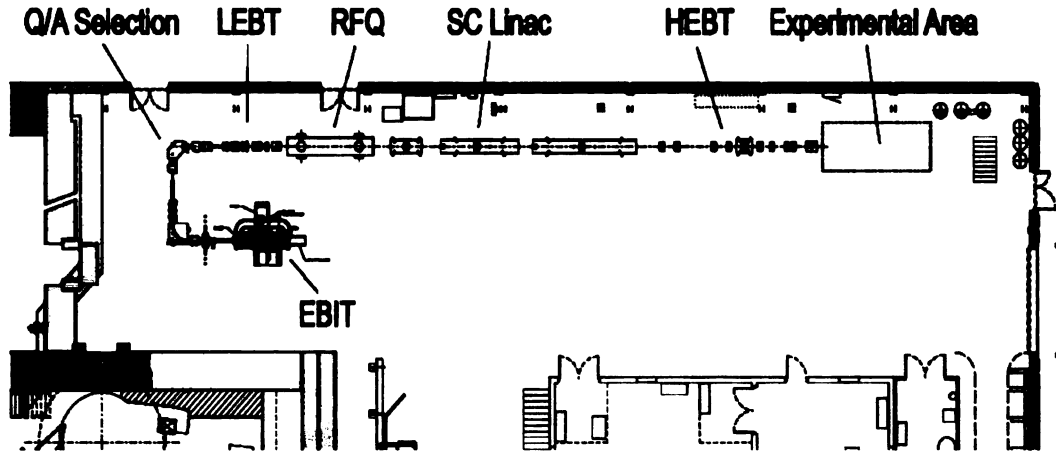


Figure 3.1. Scheme of the EBIT-based  $N^+$  reacceleration under development at the NSCL [29].

## 3.2 Status of the charge breeder at the NSCL

The design of several parts of the EBIT and its support structure vacuum and electronic system is completed. Extensive simulations have been performed to understand and optimize the electron gun optics and electron beam properties. Construction of some components has started and the EBIT is expected to be ready for first tests in 2009.

### 3.2.1 Electron gun

The assembly of the electron gun is nearly completed. Design work was supplemented with simulations to achieve the desired features needed for an efficient operation of the EBIT. The electron gun was designed in such a way that different cathode options can be

implemented giving different electron currents. A high current is very important for the EBIT, since it will increase the current density inside the trap, thus improving the charge breeding speed. A section view of the electron gun is given in Figure 3.2.

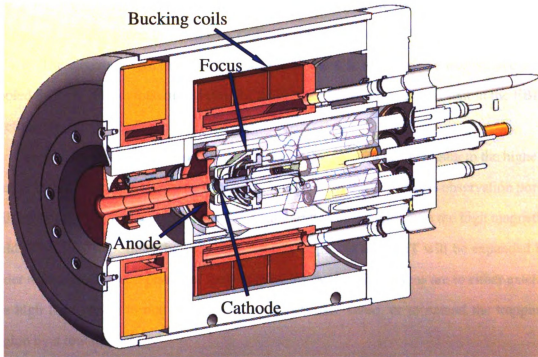


Figure 3.2. Section view of the electron gun assembly. The cathode emits electrons that are accelerated and extracted through the anode.

The electrostatic components of an electron gun include the cathode, focus and anode electrodes. The parts of the magnet include the bucking coil, the trim coil and the soft iron.

The electrons are produced in the cathode which is enclosed by the focus electrode assisting in the tuning of the beam current. The electrons are accelerated and extracted through the anode.

The purpose of the soft iron is to shield the cathode region in the electron gun from the fringe fields of the EBIT's magnetic field. The bucking coil produces a magnetic field that eliminates the remaining field at the cathode. This is very important, since the electron

beam radius inside the EBIT critically depends on the magnetic field at the cathode  $B_c$ , and by reducing  $B_c$  it is possible to obtain a higher compression of the beam (see Equation 2.1).

### 3.2.2 Trap

The axial electric trapping field will mainly be provided by a number of near-cylindrically shaped electrodes. Since the magnetic coils are superconducting, they have to be cooled to 4 K. The electrodes are in thermal contact with the 4 K shield of the magnet and also cooled down to this temperature giving the advantage that residual gas present in the EBIT is efficiently suppressed.

The NSCL charge breeder requires a high magnetic field for fast breeding to the highest charge states. Since it is desirable to observe X-rays from the trap, radial observation ports will be installed. This requires a split-coil configuration which produces the high magnetic field of up to 6 T. Besides the split coils the trap region in the EBIT will be expanded in order to increase the acceptance of the incoming ion beam. The options are to either extend the high field region to one side, giving an 'EBIS-like' setup, or to extend the trapping region by a low field.

The idea to include a low-field region in the EBIT is motivated by the fact that lowering the magnetic field will make the electron beam wider. Since some ions of the beam have larger orbiting radii, they can spend more time inside the electron beam thus possibly increasing the ionization probability. After the ionization in the wide electron beam, the orbiting radius of the ion will decrease, so that it will spend more time inside the electron beam even if the beam is more compressed. This way further ionizations can occur in the high-field region.

However, since it is not obvious whether a low-trap region would benefit over a high-field region with its higher current density, numerical studies have been performed in this work to answer this question.

### 3.2.3 Collector

The collector is nearly assembled, and a section view is given in Figure 3.3. After passing through the trap the electrons are collected on the surface of the collector. The design of the collector allows for electron beam currents of up to 5 A, and with final beam energies of up to 2 keV. This gives a dissipated power of 10 kW, while thermal studies predict that powers up to 30 kW can be dissipated.

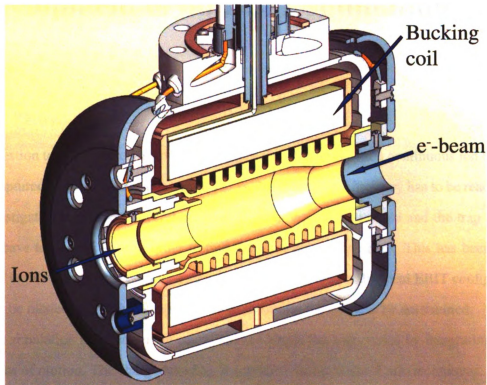


Figure 3.3. Section view of the collector assembly.

## Chapter 4

# Development of an EBIT simulation code

The question to be answered is how to maximize the probability for a continuous ion beam to be captured in an EBIT. For this a high  $1+ \rightarrow 2+$ -ionization efficiency has to be reached. To investigate this problem several configurations in the magnetic field and the trap electrodes have to be looked at in order to find the most promising setup. This has been addressed in this work by developing a simulation code that allows different EBIT configurations to be modelled and the acceptance of an incoming ion beam to be determined.

The simulation is based on the calculation of single ion trajectories by integrating the equations of motion. The charge breeding is modelled using Monte Carlo techniques. This allows one to simulate multiple ionization steps, since the stochastic nature of the processes is preserved. Single ion simulations are repeated for a representative number of ions that constitute an ion beam.

Not included in the model are ion-ion or ion-electron interactions besides electron impact. Space charge effects resulting from the ions were also neglected.

## 4.1 Simulation algorithm for ion dynamics

To obtain realistic predictions of the code, it is important to have a reliable algorithm that describes the ion dynamics. An efficient algorithm exhibits precision while at the same time allowing short computational times. To compare the performance of different algorithms, a test case was implemented with parameters similar to those used in the actual simulation. The test case considers an ion that is confined inside an electron beam in the two-dimensional transverse plane. A homogeneous magnetic field is used. An analytical solution exists for this case, so that the results given by different algorithms can be compared. The parameters  $B = 6$  T,  $r_H = 50$   $\mu\text{m}$ ,  $r_T = 3$  mm and the initial injection conditions  $r_{in} = 25$   $\mu\text{m}$ ,  $v_r = 63222$  m/s,  $v_\phi = 0$  m/s were used for the test case. It could be observed that the adaptive fourth-order Runge-Kutta algorithm [30] shows good results and was chosen for the integration of the equations of motion. The root mean square of the error in the position of the ion is around  $2.0 \cdot 10^{-7}$  m, when compared to the exact solution for an orbit period after a time of  $t = 5$  ms, which is a long time-scale when compared to ion capture processes.

## 4.2 Trap setup

Figure 4.1 shows a sketch of the electrode system and coil configuration of the trap as considered in the simulations. The setup is largely based on the TITAN setup [15] with the modification that a longer trapping region is implemented. The design study includes two regions, where different magnetic fields can be applied. Since a high magnetic field is required to charge breed the ions into the highest charge states, one of the two regions has to provide this high field. This region is labelled ‘trap’. The other region, labelled ‘post-trap’, has the purpose to increase the acceptance for the incoming ion beam. Further ionization of the captured ions would then predominantly occur in the high-field ‘trap’ region. The magnetic field in the ‘post-trap’ region can be varied in order to study the

effect on acceptance. Moreover, it is possible to change the sequence of both regions, so that the 'post-trap' becomes a 'pre-trap'.

The variation of the radius of the electrodes was included in the code to realistically model the space charge potential according to Equation 2.3. The voltage between adjacent electrodes is approximated linearly thus giving a constant electric field over the gap region.

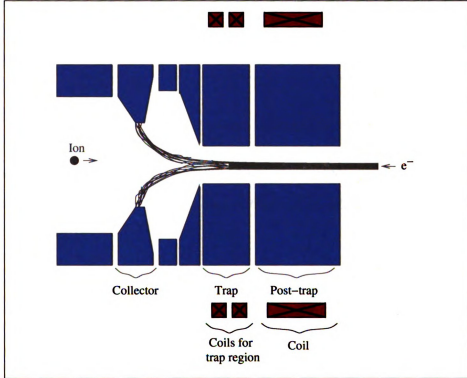


Figure 4.1. Schematic view of the EBIT setup as used in the code, not to scale.

The magnetic field is generated by several coils. The axial magnetic field of a single coil is described by [31]

$$B_{z,r=0} = \frac{\mu_0 I n}{2(r_2 - r_1)} (z - z_2) \ln \frac{\sqrt{r_2^2 + (z - z_2)^2} + r_2}{\sqrt{r_1^2 + (z - z_2)^2} + r_1} - \frac{\mu_0 I n}{2(r_2 - r_1)} (z - z_1) \ln \frac{\sqrt{r_2^2 + (z - z_1)^2} + r_2}{\sqrt{r_1^2 + (z - z_1)^2} + r_1} \quad (4.1)$$

with  $\mu_0$  as the vacuum permeability,  $I$  as the current flowing through the coils,  $n$  as the number of turns per length.  $r_1$ ,  $r_2$ ,  $z_1$  and  $z_2$  are specified in Figure 4.2.

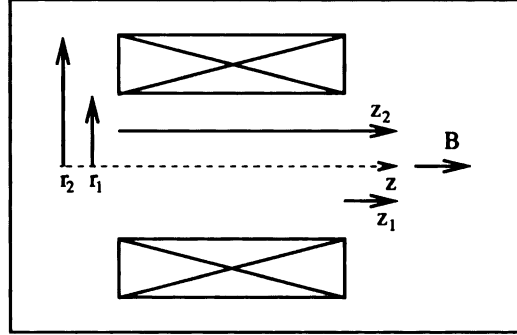


Figure 4.2. Illustration of a finite sized solenoid used to calculate the axial magnetic field.

Since the radii of the ions are small in the EBIT, the dependence of  $B_z$  on  $r$  is neglected. By changing the current  $I$  for the coils used, different magnetic field configurations can be created for the EBIT.

### 4.3 Ionization

The mechanism of charge breeding is implemented using a Monte Carlo approach in order to consider the statistical nature of the ionization process. For the top-hat electron beam considered in the code two situations can be distinguished as discussed in Section 2.1. The ion is either inside the constant charge density electron beam or it is outside.

Following every step it is determined, if the ion is inside the electron beam or not, since only in the first case there is a non-vanishing probability for ionization. If the ion is inside the electron beam, the time-interval since the last integration step is used to assign a probability  $p$  for ionization with Equation 2.15. The time-interval between two integration steps is typically of the order  $\Delta t \approx 10^{-10}$  s. The probability  $p$  is compared to a generated random number  $n \in [0, 1]$ , and if  $p > n$  holds true, the ion changes its charge state to  $q \rightarrow q + 1$ .

The parameters needed for the calculation of the Lotz cross-sections with Equation 2.14 are taken from [32–35].

## 4.4 Capture of ions

Since the code has to evaluate the trapping efficiency, a suitable definition for ion capture is needed. Even though it is desirable that an ion is captured every time when it undergoes an ionization from the singly charged to the doubly charged state, practically this is not always the case. For example, it is possible that an ion is ionized before reaching the potential barrier at the entrance of the trap and will be reflected. For this reason the condition of a  $1+ \rightarrow 2+$ -ionization step is insufficient for the capture of an ion.

A different indicator for a capture could be that the ion changes the direction of its axial movement twice: Once when being reflected by the potential barrier at the end of the trap and a second time by the potential barrier at entrance.

In the simulation both criteria have to be fulfilled for an ion to be considered captured.

## 4.5 Injection of ions

Figure 4.1 shows that external ions are injected through the collector. Ideally there should be no magnetic field at the collector, so that the beam can maximally diverge when being collected on the inner face. However, since this case is difficult to implement in the simulation realistically, a small but finite magnetic field of about 10 G exists at the collector. This way, there is a finite electron beam radius, which introduces a discontinuity in the potential. The magnitude of the discontinuity depends on the radial distance from the center of the electron beam as can be seen in the formula for the space charge potential in Equation 2.3. To solve the problem with the discontinuity in the potential, the depth of the space charge potential  $U_d$  is calculated at the collector for  $r = 0$  and a linear potential decrease is introduced to compensate for the discontinuity. Since the exact value of the

discontinuity depends on the radial position of the ion when it reaches the collector, the difference between  $U_d$  and the actual space charge potential is computed. This difference is taken into account by changing the axial velocity in such a way that the total energy is conserved.

## 4.6 Evaluation of axial potential

The equations of motion have to include the space charge potential due to the electron beam. The equations for the radial coordinates are given by Equations 2.5-2.8 and the axial equation of motion is determined by the electric field resulting from the space charge (Equation 2.10) and the applied voltages. To calculate Equation 2.10, we first note that the quantities  $Q_e$ ,  $r_H$  and  $r_T$  depend on the axial position  $z$ . Thus we can write

$$E_{z,el} = -\frac{\partial Q_e}{\partial z} \cdot \frac{1}{2\pi\epsilon_0} \left[ \frac{1}{2} \left( 1 - \frac{r^2}{r_H^2} \right) + \ln \left( \frac{r_T}{r_H} \right) \right] \quad (4.2)$$

$$-\frac{\partial r_H}{\partial z} \cdot \frac{Q_e}{2\pi\epsilon_0} \left( \frac{r^2}{r_H^2} - \frac{1}{r_H} \right) \quad (4.3)$$

$$+\frac{\partial r_T}{\partial z} \cdot \frac{Q_e}{2\pi\epsilon_0} \frac{1}{r_T} \quad (4.4)$$

for  $r \leq r_H$  and

$$E_{z,el} = -\frac{\partial Q_e}{\partial z} \cdot \frac{1}{2\pi\epsilon_0} \ln \left( \frac{r_T}{r} \right) - \frac{\partial r_T}{\partial z} \cdot \frac{Q_e}{2\pi\epsilon_0} \cdot \frac{1}{r_T} \quad (4.5)$$

for  $r_H < r \leq r_T$ . The derivatives  $\frac{\partial Q_e}{\partial z}$ ,  $\frac{\partial r_H}{\partial z}$  and  $\frac{\partial r_T}{\partial z}$  are evaluated numerically with the two-point backwards formula as

$$f'(z_i) = \frac{f(z_i) - f(z_{i-1})}{z_i - z_{i-1}}, \quad (4.6)$$

$f$  being the quantity that is to be derived,  $z_i$  being the position at time-step  $t_i$  and  $z_{i-1}$  at time-step  $t_{i-1}$ .

## 4.7 Electron beam energy

The electric field produced by the space charge potential and considered for the ion dynamics has been discussed in Section 2.2. The dynamics of the electrons is influenced by their own space charge potential. Thus a self-consistent potential calculation is in principle needed to properly include space charge effects. Since this requires substantial computational time, as a starting point only the potential produced by the electrodes was considered. The consequence is that the electron beam energy used in the simulations is somewhat overestimated. The difference is approximately equal to the space charge potential.

The electron beam energy  $E_e$  is needed for the Brillouin radius given by Equation 2.2 and the Lotz cross-sections as can be seen from Equation 2.14. However, since  $E_e$  enters as  $E_e^{1/4}$  in Equation 2.14, its effect on the electron beam radius is small, and thus the approximation is valid for this case. Considering the cross-sections for ionization, it will be shown later that the capture probability does not differ greatly for varying electron beam energies. For this reason the approximation used is also reasonable for the ionization process.

One way to include self-consistent effects efficiently would be to calculate the potential distribution of an electron beam beforehand, and then include it in the calculations. This way it is not needed to calculate space charge effects during the actual simulation.

## 4.8 Other simulation parameters

The values of parameters that are kept fixed in the simulations are specified in Table 4.1. The values are similar to values used in literature for similar work [7,26]. Iron ions ( $Z=26$ ) are used for all of the simulations, unless noted otherwise. For maximum compression of the electron beam a zero magnetic field is needed at the cathode. Simulation work for the electron gun showed that the magnetic field at the cathode can be reduced to a value of  $B_c = 10$  G or even lower.

The radii of the magnetic coils  $r_{in}$  and  $r_{out}$  are taken to be the same as the coil dimen-

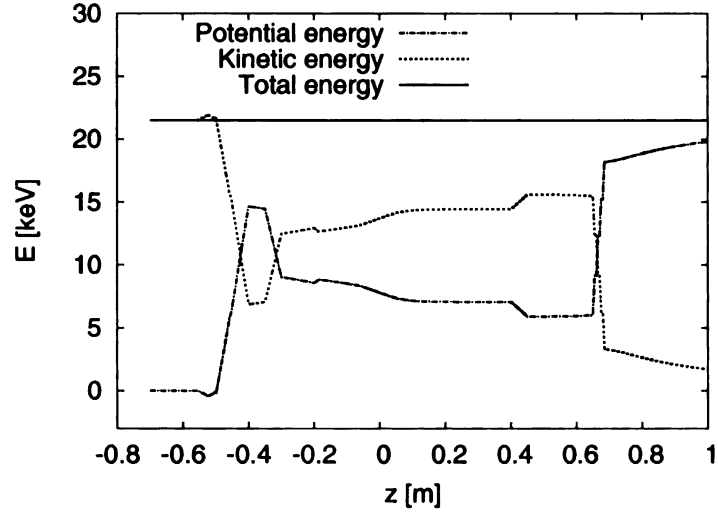
sions used at TITAN. The value of the cathode radius  $r_c$  is also taken from TITAN which uses a  $I_e = 0.5$  A electron gun. Since the NSCL charge breeder will use a higher current electron gun, the cathode radius is larger by a factor of 2-4. The consequence is that the electron beam is wider, if other parameters are kept constant.

Parameter		Value
Magnetic field at cathode	$B_c$	10 G
Cathode temperature	$T_c$	1400 K
Cathode radius	$r_c$	1.5 mm
Inner radius of magnetic coils	$r_{in}$	57.5 mm
Outer radius of magnetic coils	$r_{out}$	108 mm
Atomic number (iron)	$Z$	26
Mass of ion	$m$	56 u

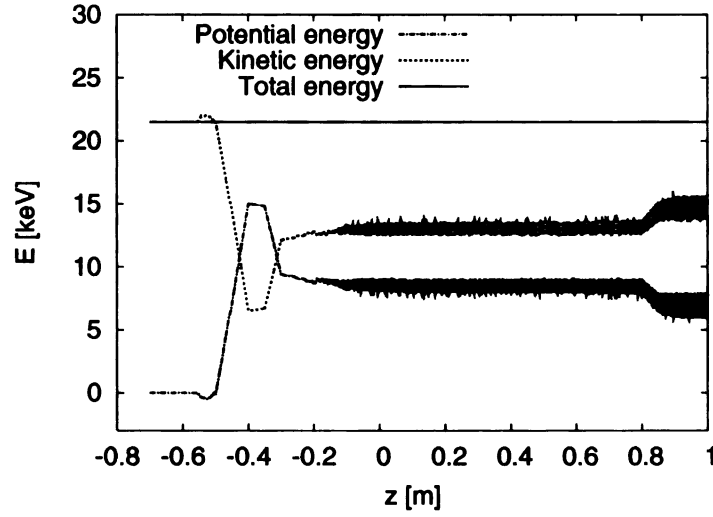
Table 4.1. Common parameters used in the simulation.

## 4.9 Code test by energy conservation

It is possible to check whether all parameters relevant to electric forces were included correctly in the code. This can be done by considering energy conservation, since the potential energy is calculated completely *analytically*, whereas the kinetic energy is calculated *numerically*. If the total energy is conserved, we know that the electric forces were handled correctly, especially with regard to the space charge potential. Figure 4.3 shows plots of potential, kinetic and total energy as a function of axial position  $z$  for two cases of ion injection, one in which an ion that is injected on-axis, and another with off-axis injection. While the details of the specific setup will be discussed later, it can be observed that the total energy is well conserved implying that the code is correct. The relative maximum deviation from energy conservation is less than  $2 \cdot 10^{-5}$ . The oscillations in the off-axis case result from the radial movement of the ion due to the space charge potential provided by the electron beam.



(a)



(b)

Figure 4.3. Test if code correctly handles electric fields due to applied and space charge potential. The figure shows the analytically calculated potential energy, the kinetic energy from the integration of the equations of motion and the sum. In (a) the ion is injected on-axis with no transverse velocity. In (b) the ion is injected at  $r_{in} = 1 \cdot 10^{-3}$  m,  $v_r = 13851$  m/s and  $v_\phi = 0$  m/s.

# Chapter 5

## Acceptance calculations

Acceptance calculations allow one to determine the capture probability for the ion beam injected into an EBIT as a function of its emittance. The code described in the previous chapter is used for these calculations.

### 5.1 Determining the capture probability

An ion starting at the displacement  $r_{in}$  from the center of the electron beam with the radial velocity  $v_r$  and the azimuthal velocity  $v_\phi$  is injected into the system. As discussed earlier two situations can occur; the ion is either captured or lost.

1. An ion is considered captured, if it changes the direction of its axial movement twice and has been ionized at least once.
2. An ion is considered lost, if
  - the ion arrives at the same axial position from where it started after having been reflected either by the first potential barrier before entering the trap or by the second potential barrier at the electron gun.
  - it hits the electrode wall.

- it changes its axial direction twice without being ionized.

For the simulation  $r_{in}$ ,  $v_r$  and  $v_\phi$  are varied on a discrete three-dimensional grid with  $N_r = 20$ ,  $N_{v_r} = 21$  and  $N_{v_\phi} = 21$  different, equidistant values. The range of the variables is  $r < 4.75$  mm and  $|v_r, v_\phi| < 5870.18$  m/s. This range allows one to probe the acceptance of the EBIT for beam emittances up to  $48 \pi \cdot \text{mm} \cdot \text{mrad}$  at 9.6 keV.

$N_{MC} = 20$  runs are used for every set of starting conditions, so that 176400 runs have to be completed for the whole simulation. The CPU time needed on a Unix machine to complete such a simulation is about 24-36 hours.

## 5.2 Acceptance

The conditions of the injected ion are given in radial coordinates due to the cylindrical symmetry of the problem. In order to visualize the results, they are transformed into the two-dimensional cartesian phase-space  $x$ - $x'$  defined in Chapter 2.6 because of the greater familiarity with emittance given in cartesian coordinates. Because of the axial-symmetry of the setup, the choice of  $x$ - $x'$ -space is arbitrary and same results are obtained in  $y$ - $y'$ -space.

A procedure as depicted in Figure 5.1 was used to obtain the acceptance in the  $x$ - $x'$  phase space for the capture results that were obtained in radial coordinates. The general loop described in the flow chart is repeated  $N_{RA} = 10^8$  times to obtain a smooth probability distribution.

The result gives the acceptance in  $x$ - $x'$  phase space. This acceptance can be called relative, because the  $x$ - $x'$ - $y$ - $y'$  phase-space has a certain volume. By changing this volume the average ionization probability for a certain point in  $x$ - $x'$  space will change. So if one increases the size beyond the area offering non-zero probabilities, the probability  $P$  for a point in phase-space will decrease. However, it is still possible to compare acceptance plots of different configurations if the phase space volume is taken to be the same. An example of an acceptance plot is given in Figure 5.2.

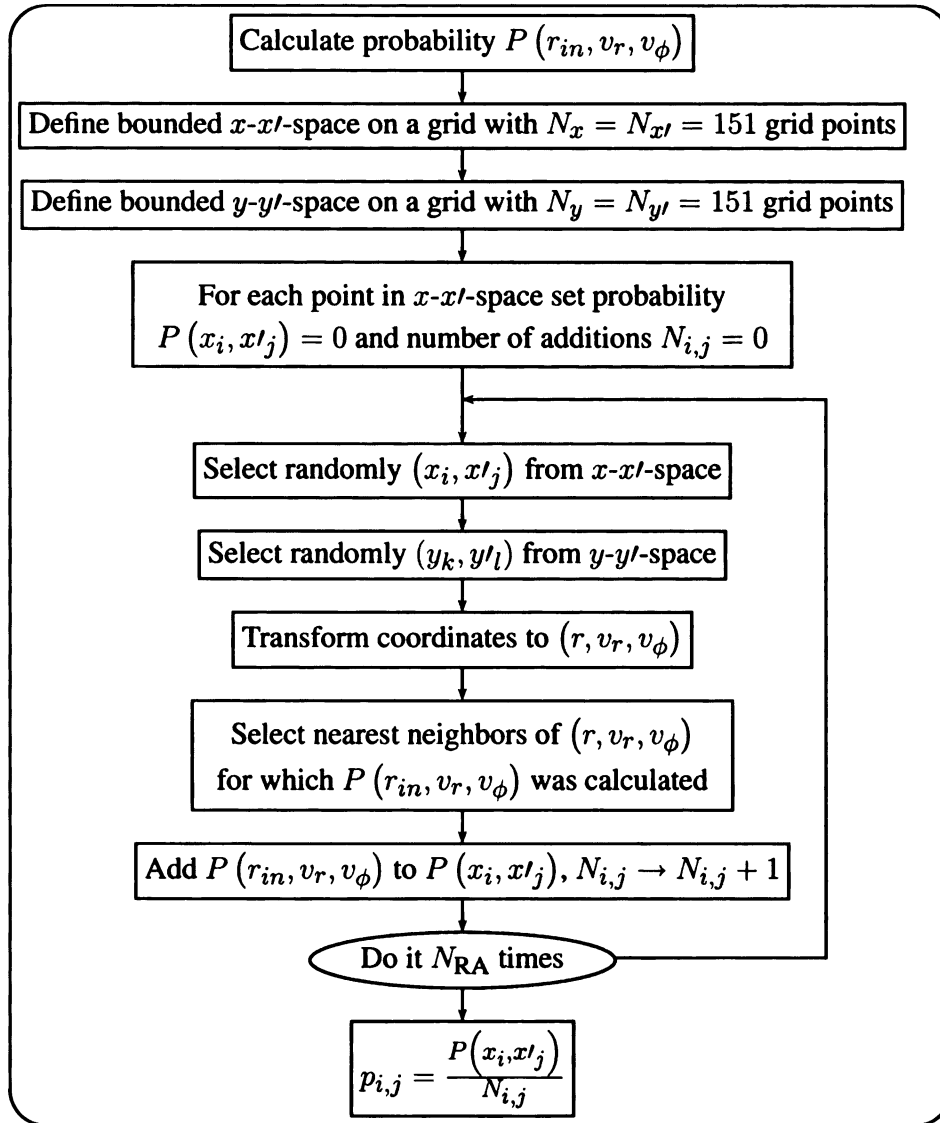


Figure 5.1. Flow chart for the acceptance calculation.

### 5.3 Capture probability

While the acceptance allows one to qualitatively compare the efficiencies of different configurations, an absolute value for the capture efficiency of a certain configuration with a certain incoming beam is needed. The efficiency of the capturing process in an EBIT is determined by the overlap of the acceptance of the trap with the emittance of the incoming beam as illustrated in Figure 2.6. By changing the emittance in the overlap calculation, one

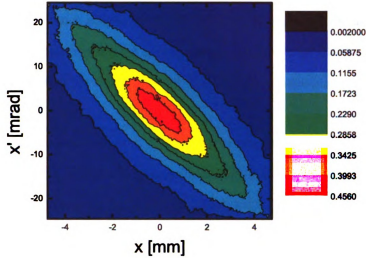


Figure 5.2. Example of an acceptance plot calculated for  $|x| < 4.75$  mm and  $|x'| < 25$  mrad. The configuration used is the '1T-6T'-configuration, described in Section 6.1

can obtain the capture probability as a function of emittance.

To obtain optimum overlap the shape of the emittance of the incoming ion beam should resemble the acceptance. Figure 5.2 illustrates that an elliptical shape of the emittance promises to offer a good overlap. For this reason a tilted ellipse is chosen to model the emittance. Different emittance values are obtained by changing the area of the ellipse while keeping the aspect ratios of both half-axes of the ellipse constant. To simplify the computational procedure, the tilted ellipse chosen to model the emittance is transformed into an upright ellipse by the following transformation

$$\begin{pmatrix} x_{\text{new}} \\ x'_{\text{new}} \end{pmatrix} = \begin{pmatrix} 1 & 0 \\ -m & 1 \end{pmatrix} \cdot \begin{pmatrix} x \\ x' \end{pmatrix}, \quad (5.1)$$

with  $(x, x')$  being the old coordinates,  $(x_{\text{new}}, x'_{\text{new}})$  being the new coordinates and  $m$  being the slope of the tilted ellipse. Using this transformation for points enclosed by the

tilted ellipse gives transformed points that are enclosed by an upright ellipse with one of its half-axes aligned with the  $x$ -axis and the other one aligned with the  $x'$ -axis.

The slope of the emittance ellipse can be determined by scanning the acceptance plot from  $x_{\min}$  to  $x_{\max}$ , and determining the  $x'$  value for a specific  $x$  that has the largest acceptance. The resulting graph of  $x'$  over  $x$  is fitted with a linear interpolation, and the slope of this curve is equaled to the slope  $m$  of the ellipse.

The ratio between the two half-axes of the upright ellipse is determined by obtaining the probability distributions of the acceptance for  $x'$  for the case when  $x = 0$  and for  $x$  for the case when  $x' = 0$ . The standard deviation is calculated for both distributions. The ratio of the standard deviations gives the ratio of the half-axes  $h_x$  and  $h_{x'}$  of the upright ellipse that is used to model the emittance of the incoming beam. The emittance of the beam is

$$\epsilon = \pi \cdot h_x \cdot h_{x'}. \quad (5.2)$$

The procedure shown in Figure 5.3 is used to obtain the capture probability as a function of the emittance of the incoming beam. The main loop is performed  $N_{\text{CP}} = 10^7$  times. In order to obtain the capture probability as a function of emittance, the procedure is repeated for ellipses with different area sizes, but same aspect ratios.

The calculations are performed up to an emittance of  $\epsilon = 48 \pi \cdot \text{mm} \cdot \text{mrad}$  at 9.6 keV. The value is considerably larger than the value of  $18 \pi \cdot \text{mm} \cdot \text{mrad}$  at 2 keV obtained experimentally for the NSCL beam cooler and buncher used for high-precision mass experiments [36], which corresponds to about  $8 \pi \cdot \text{mm} \cdot \text{mrad}$  at 9.6 keV. Since similar beam cooling is performed after the NSCL gas stopper, the emittance range is large enough to cover any likely beam scenario.

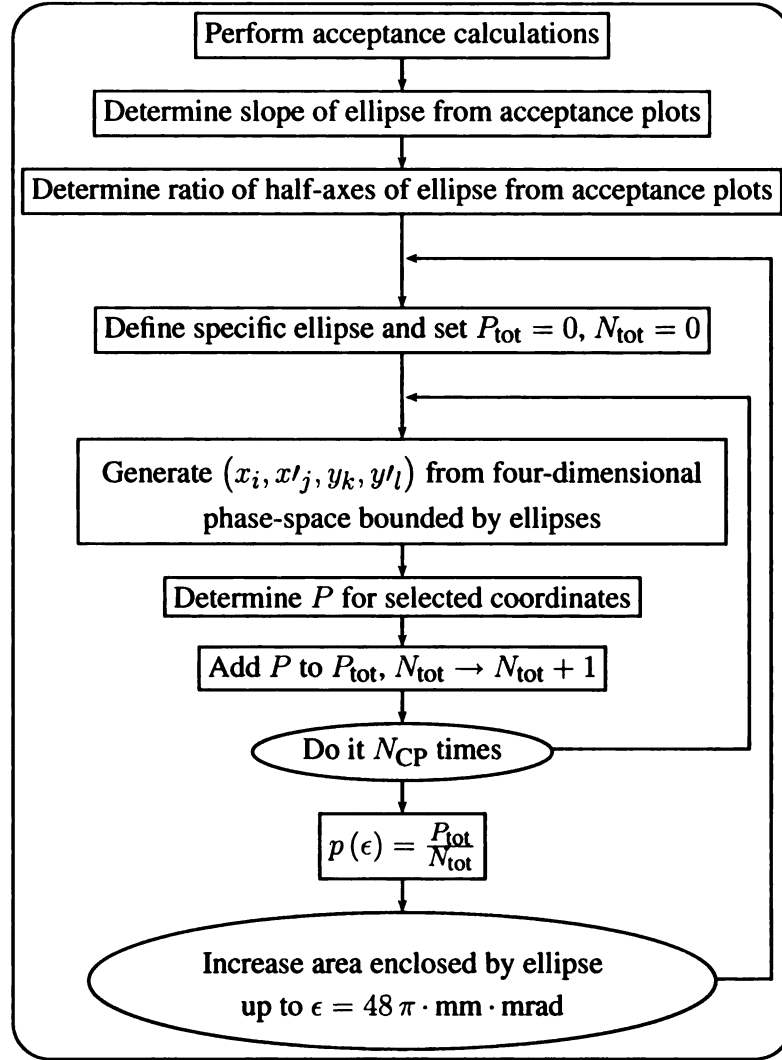


Figure 5.3. Flow chart of the capture probability calculation.

# **Chapter 6**

## **Investigation of different field configurations for the NSCL charge breeder**

The performance of the NSCL charge breeder will depend on a multitude of parameters. Some combinations of these parameters are ideal for charge breeding of ions into the highest charge states. Other combinations give a better capture probability of the injected ion beam. The goal of studying different possible configurations is to find a configuration that optimizes capture, but also offers the potential for fast charge breeding.

### **6.1 Magnetic field**

For the trap to be able to charge breed ions into high charge states, a high current density is necessary as can be seen from Equations 2.15 and 2.16. By guiding the electron beam from the cathode ( $B \approx 0$  T) into a region with a strong magnetic field, the radius of the electron beam shrinks and the current density  $j$  grows (see Equation 2.16). For this reason a high magnetic field is required in the trap region where the ions are to be charge bred to

the highest states. A potential disadvantage of the high magnetic field and the associated smaller electron beam radius comes from the fact that injected ions might orbit with larger radii compared to the electron beam radius. In such a case a compressed electron beam might result in a poor overlap between the ions and the electron beam causing a decrease of the ionization probability.

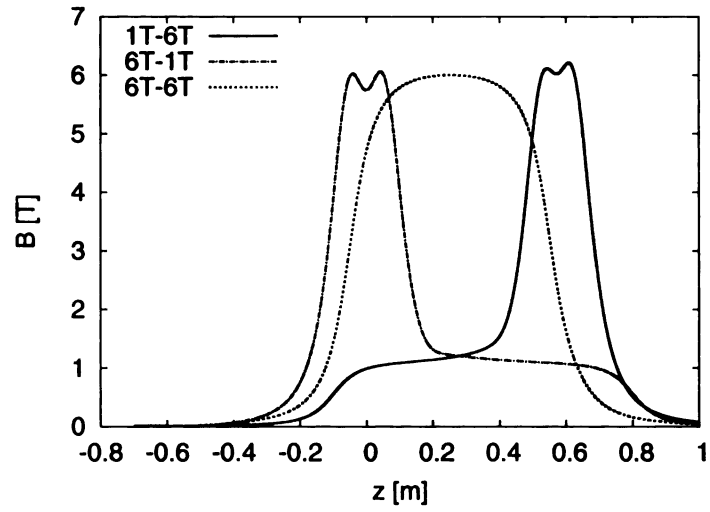
By lowering the magnetic field the electron beam will become wider, so that ions with larger orbiting radii can spend more time inside it, possibly favoring ionization. In order to incorporate this idea, a low field region can be introduced besides the high field region: After the injection, ions could be ionized in the wide electron beam in the low field region leading to their capture. Following the initial ionization in the wide electron beam, the average radius of the ions will decrease because of their higher charge state. In this way, the time ions spend inside the electron beam is increased. A high-field region could then be used for fast ionization to the desired maximum charge state.

This idea can be realized in the EBIT by implementing an additional low-field region before or after the high field trap region. While appearing promising, it is not certain whether such a configuration benefits over a configuration with the same dimensions where a high magnetic field is prevalent everywhere.

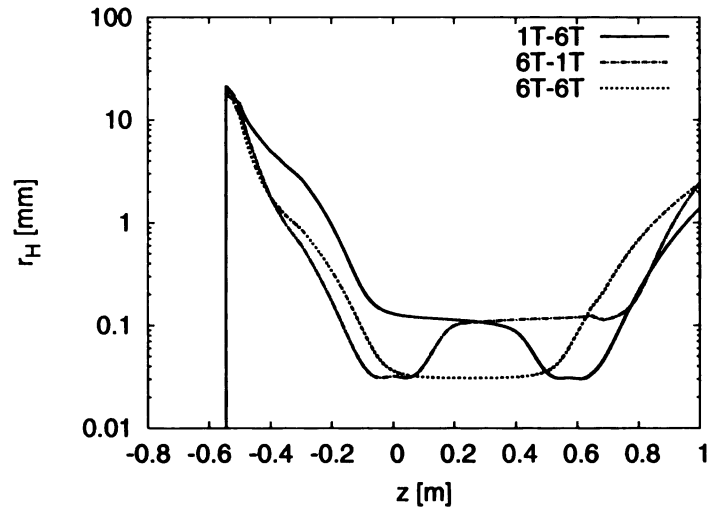
Within this work different configurations have been analyzed and their capturing efficiencies have been quantified. Three basic configurations have been considered as shown in Figures 6.1 and 6.2.

- ‘6T-1T’-configuration: It features a short magnetic high-field region (6T) facing the collector and an extended low-field (1T) region on the electron gun side.
- ‘1T-6T’-configuration: It includes a high-field (6T) and a low-field (1T) region, but their positions are swapped compared to the situation above.
- ‘6T-6T’-configuration: It features a peak magnetic field around 6T throughout the full length of the trap.

The dimensions of the coils that produce these magnetic fields are given in Table 6.1.

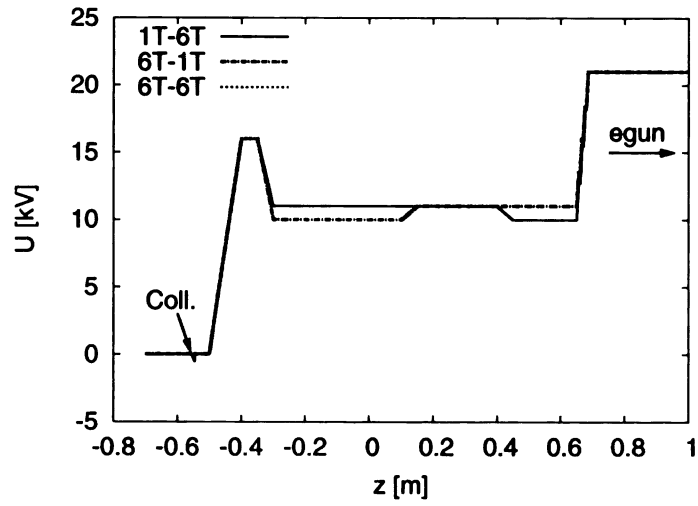


(a)

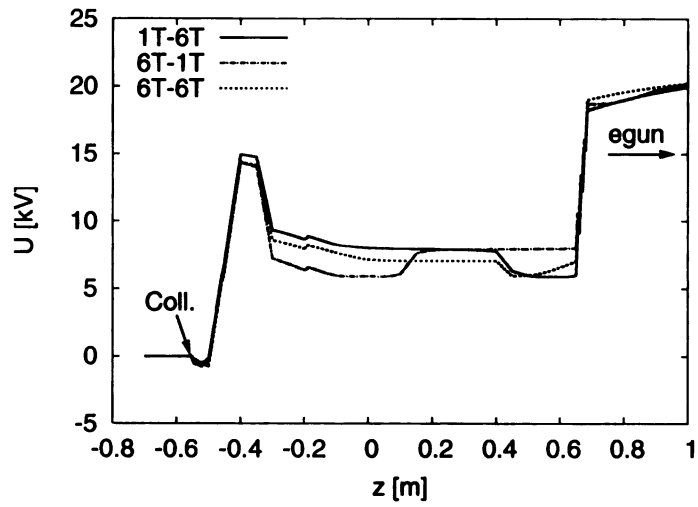


(b)

Figure 6.1. Comparison between three magnetic field configurations (a). Corresponding electron beam radii as given by the Herrmann radius  $r_H$  (b)



(a)



(b)

Figure 6.2. Axial potential for different magnetic field configurations. Top: Potentials obtained from applying voltages to the electrodes. Bottom: Potentials including space charge effects.

	$z_{\text{begin}}$ [m]	$z_{\text{end}}$ [m]	$\mu_0 I n/2$ [T]
<b>'6T-1T'</b>			
Coil 1	-0.0835	-0.02725	0.662
Coil 2	0.02725	0.0835	0.662
Coil 3	0.2	0.8	0.05
<b>'1T-6T'</b>			
Coil 1	0.5	0.55	0.7
Coil 2	0.6	0.65	0.735
Coil 3	-0.1	0.4	0.05
<b>'6T-6T'</b>			
Coil 1	-0.05	0.5	0.283

Table 6.1. Dimensions of the coil configuration, and the pre-factors from Equation 4.2 for the different magnetic field configurations

## 6.2 Potential configuration and electron beam energy in the trap

The potential configuration in an EBIT can be changed by applying different voltages on the electrodes. Since ions are injected through the collector with an energy of several keV, a first potential barrier is introduced shortly after the collector to slow them down. To allow the ions to perform a round-trip in the trap, a second potential barrier is set up before the electron gun. The potential of this barrier is chosen to be large enough, that all ions are reflected. A potential well between both barriers ensures that if the ion is ionized, it will be captured. An example of the potential configuration, with and without space charge, and of the magnetic field is shown in Figure 6.3.

It is apparent that the space charge contributes significantly to the potential. By modifying the compression of the electron beam with a change in the magnetic field, the space charge potential changes, so that the ion feels an additional electric field resulting from the space charge. By changing the voltages on the electrodes, the electron beam energy is modified, and thus the velocity of the electrons also changes, which then effects the

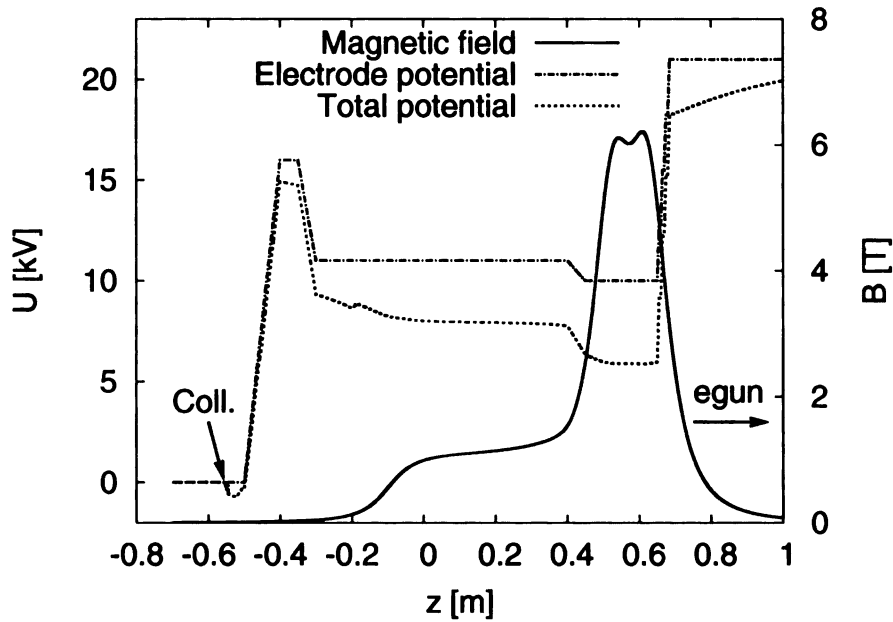


Figure 6.3. Potential and axial magnetic field configurations on axis. The different curves show the potential produced by the electrodes (dot-dash), the total potential including space charge effects (dot) and the magnetic field (solid). The electron beam current is  $I = 2.5$  A.

potential.

It is important to consider the radial dependence of the space charge potential as given by Equation 2.3 when using the approximation for adjusting the axial energy at the collector as described in Section 4.6. Ions that enter through the collector at relatively large radial displacements are not accelerated as strongly as ions entering near the electron beam axis.

Depending on the position of the first potential barrier and the electron beam density in its vicinity, there are ions that are ionized before reaching this barrier, and thus they can be reflected and get lost. This could become important if the magnetic fringe field extends well beyond the trap region. By analyzing how many ions are ionized in the fringe field, a prediction can be made where the barrier should be placed.

The kinetic energy of the injected *ions* has to be chosen carefully for the following reasons: If the energy is too low, the ions will be reflected by the first potential barrier even if they remain singly charged. If the energy is high, the ions will have a large axial velocity

in the trap. The consequence could be that they interact with the electron beam only for a short period of time making ionization unlikely. The space charge potential makes it more complicated to estimate the right proportion between the potential of the barrier and the axial kinetic energy, because ions passing the collector at different radii will feel different space charge potentials. So while ions moving close to the electron beam can become captured, this could mean that other ions moving far off-axis will be reflected.

It can be seen from Figure 6.2 (top) that the potential of the barriers is kept the same for all configurations. The axial energy of the injected ions is chosen to be 1.6 keV higher than the on-axis potential of the first barrier including the space charge potential.

Because of the changing potentials produced by the electrodes, the energy of the electron beam changes when it moves through the EBIT. Figure 6.4 shows the electron beam energy along the axis for conditions that correspond to the potential configuration shown in Figure 6.3. Since changing the potential in the trap allows one to choose the electron beam energy in this region, several simulations can be performed to observe the change in acceptance. Because it is desirable to finally trap the ions inside the region with the high magnetic field, a further potential well is introduced there. In this way, two extended regions with different electron beam energies can be realized. When describing a configuration with a certain electron beam energy, both electron energies in the trap will be given. For example the electron beam energy for the configuration shown in Figure 6.4 is given by  $E_e = 12 - 13$  keV.

Changing the potential in the trap enables one to select an energy that is optimal for a certain ionization step (see Equation 2.14). The most efficient energy for ionization lies at  $1.5 \times I_p$  [25] where  $I_p$  is the ionization potential for the least bound electron. This means that for the removal of the first few electrons a lower energy beam is favorable, however for breeding into higher charged states higher energies become necessary. To limit the power that needs to be dissipated in the collector a final electron beam energy of  $E_e = 2$  keV is required.

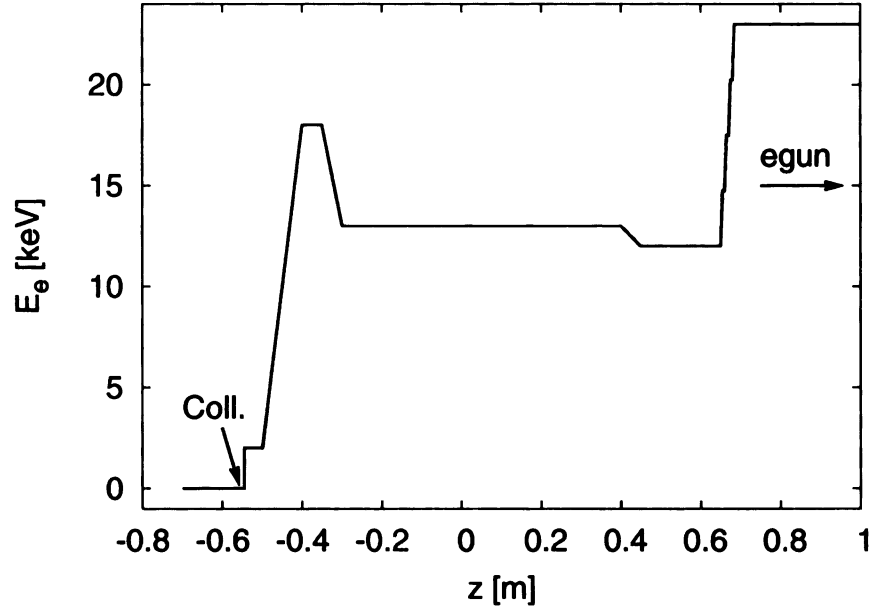


Figure 6.4. Electron beam energy distribution generated using the potential given by the voltages applied on the electrodes as specified in Figure 6.3. Space charge effects are neglected.

### 6.3 Electron beam current

The main enhancement for the ionization process is the higher current density of the electron beam as can be seen in Equation 2.16. Equation 2.3 shows that a high electron current is beneficial for the ionization process due to the increase of the depth of the potential increased by the space charge. The result is an improved radial trapping of the ions, so that they will spend more time inside the electron beam.

However, if the current density is increased, space charge effects become more dominant, and need to be considered in the calculations. This is illustrated in Figure 6.5 where the space charge potential is plotted for different electron currents, while both the magnetic field configuration and the potentials from the electrodes stay the same.

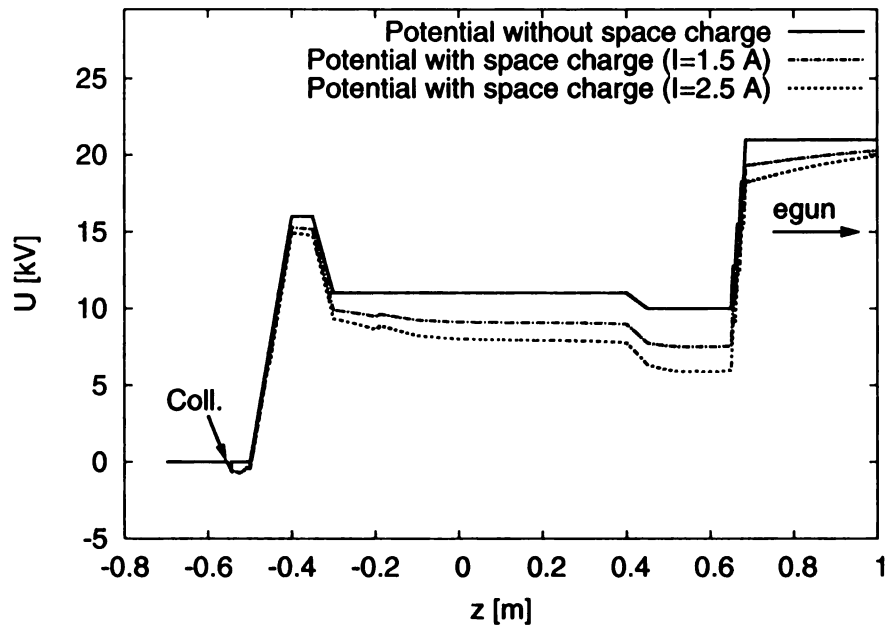


Figure 6.5. Axial on-axis potential configurations for '1T-6T' showing potential without space charge and with space charge for different electron currents.

# Chapter 7

## Results

### 7.1 Charge evolution of an injected ion

To observe the charge evolution of a single ion, a  $\text{Ti}^{1+}$  ion is injected into the ‘1T-6T’-configuration as defined in Section 6.1 at an electron beam energy of  $E_e = 10 - 11$  keV. Once the ion enters the trap, every ionization step is recorded as well as the time when it happened. The cut-off time, i.e., the time when a simulation is aborted, is  $t_{cut} = 5 \cdot 10^{-4}$  s. This time is about 28 times longer than the typical round-trip time in the trap.  $N_{MC} = 100$  Monte Carlo runs are performed.

Figure 7.1 (left) shows the calculated average times to reach a certain charge state. Figure 7.1 (right) presents the probability that the ion did actually reach this charge state. The results clearly show that for the selected EBIT configuration the first ionization occurs on the time-scale of  $\approx 10^{-6}$  s. We can see that the probability to reach charge states  $< 12$  is almost one, however subsequently it decreases rapidly, which can be explained by the decreasing ionization cross-sections for high charge states and the limited time assigned for a simulation run.

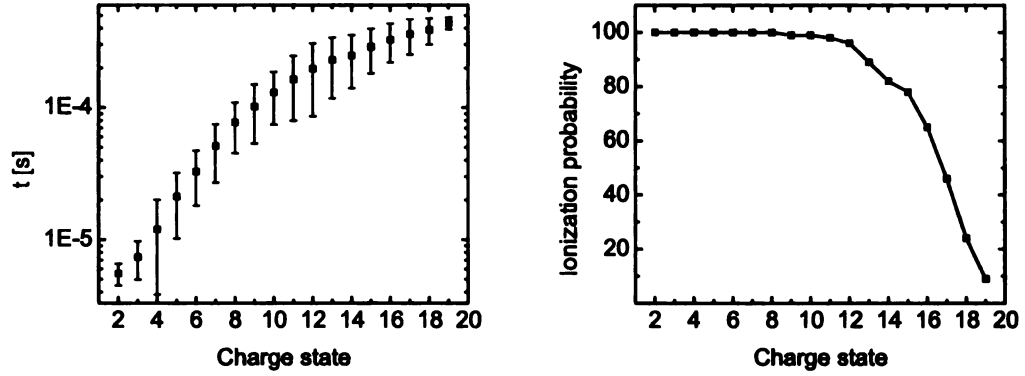


Figure 7.1. Charge evolution for a Ti-ion. The ‘1T-6T’-configuration is used with an electron energy of  $E_e = 10 - 11$  keV and an electron beam current of  $I_e = 2.5$  A. Left: Average ionization time to reach a charge state. Right: Ionization probability to reach a certain charge state within  $t_{cut} = 5 \cdot 10^{-4}$  s.

## 7.2 Magnetic field

### 7.2.1 Capture probability

Capture probability calculations were performed for the three magnetic field configurations ‘1T-6T’, ‘6T-1T’ and ‘6T-6T’ described in Section 6.1. The calculations were performed for an electron current of  $I_e = 2.5$  A, and for different electron beam energies in the trap being  $E_e = 10 - 11$  keV,  $E_e = 12 - 13$  keV and  $E_e = 13 - 14$  keV. Figure 7.2 shows the results of these calculations.

It can be observed that for  $\epsilon < 10 \pi \cdot \text{mm} \cdot \text{mrad}$  both the ‘1T-6T’ and ‘6T-6T’ configurations offer a capture probability of around one. The ‘6T-1T’-configuration offers a significantly lower capture probability over the full range of emittances. Only for a very small emittance does the capture probability approach the efficiency of the other configurations. Comparing the performance of the ‘1T-6T’ and ‘6T-6T’ configurations, it can be observed that for emittances up to around  $\epsilon \approx 15 \pi \cdot \text{mm} \cdot \text{mrad}$  the ‘6T-6T’-configuration does offer a slightly higher capture probability than the ‘1T-6T’-configuration. However, for larger

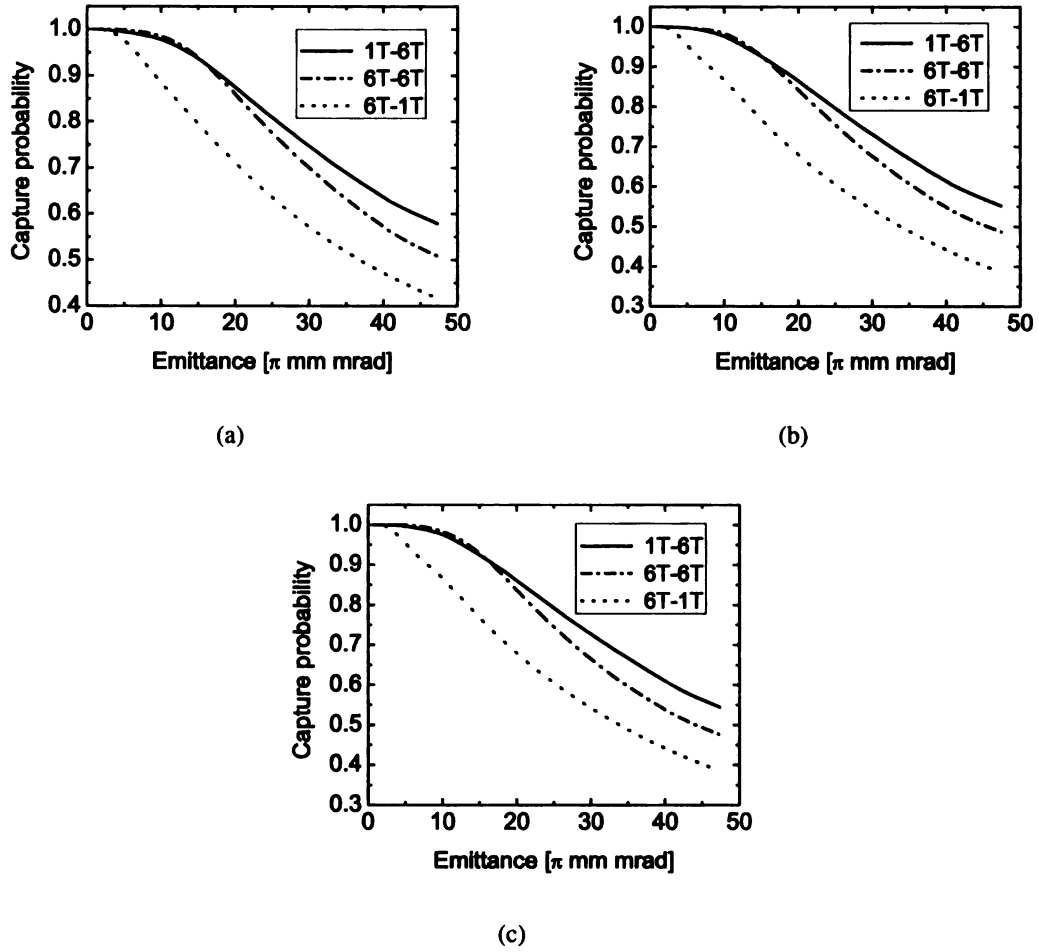


Figure 7.2. Comparison of the capture probability as a function of emittance for three different magnetic field configurations. The calculations were performed for electron beam energies of (a):  $E_e = 10 - 11$  keV, (b):  $E_e = 12 - 13$  keV and (c):  $E_e = 13 - 14$  keV in the trap. The electron current is  $I_e = 2.5$  A.

beam emittance values the '1T-6T' configuration does offer a higher capture probability.

## 7.2.2 Position at first ionization

The simulation code records when and where an ion is ionized for the first time for all ions that did undergo at least one ionization. Figure 7.3 shows histograms for the axial position of that ionization together with the magnetic field (electron beam energy is  $E_e = 12 -$

13 keV). The upper half of a histogram shows the ionization before the reflection at the second barrier. The lower half shows the ionization after the reflection.

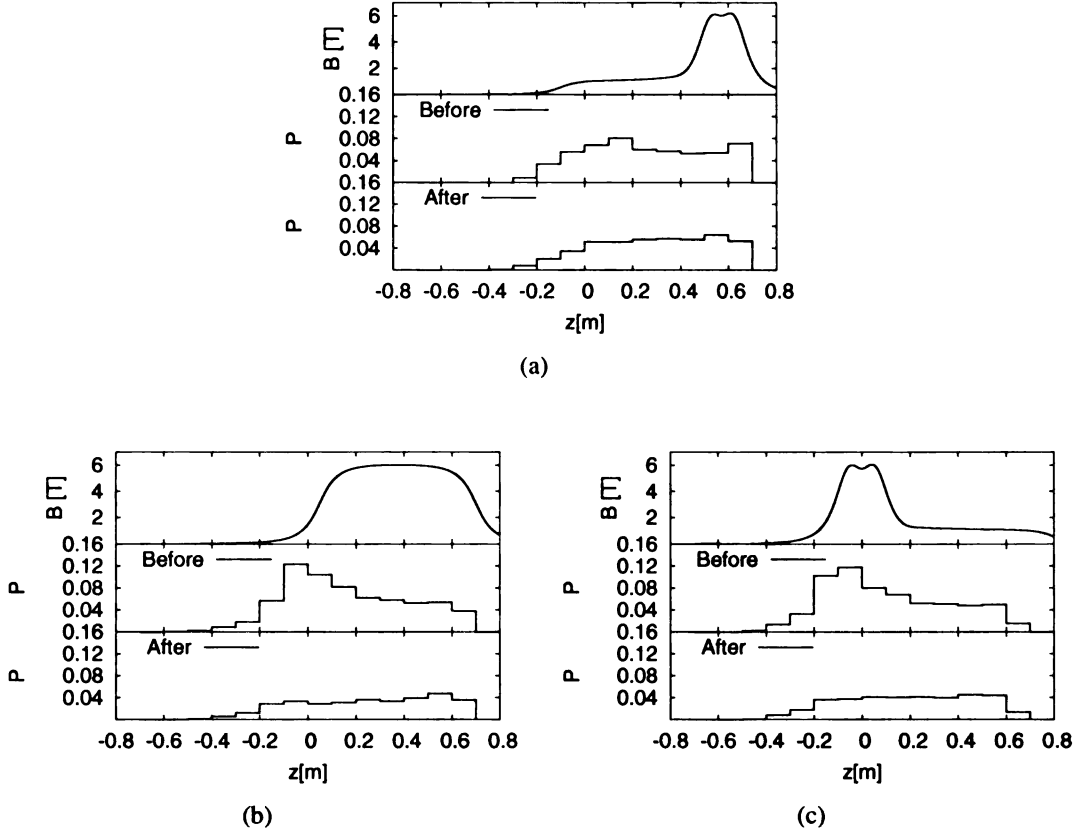


Figure 7.3. Histogram for the position of the first ionization after injection for the three configurations (a): ‘1T-6T’, (b): ‘6T-6T’, (c): ‘6T-1T’. The data is taken are the simulations with an electron beam energy of  $E_e = 12 - 13$  keV. The upper half of a histogram shows the ionization for the in-going beam. The lower half shows the percentage of  $1^+ \rightarrow 2^+$  ionization after the ions have been turned around at the second barrier.

The histograms show that for both configurations ‘6T-6T’ and ‘6T-1T’ the dominant ionization occurs for the in-going beam in the beginning of the trap between  $z = -0.2$  m and  $z = 0.1$  m, where the magnetic field reaches its peak value. Outside this region the probability for ionization decreases. For the ‘1T-6T’-configuration the distribution is almost flat in the 1T part. It rises again just before the second barrier where the magnetic field is high.

	'1T-6T'	'6T-6T'	'6T-1T'
$(E_e = 10 - 11 \text{ keV})$			
Before	63.4%	66.4%	63.1%
After	36.6%	33.6%	36.9%
$(E_e = 12 - 13 \text{ keV})$			
Before	62.8%	66.1%	63.2%
After	37.2%	33.9%	36.8%
$(E_e = 13 - 14 \text{ keV})$			
Before	62.9%	66.5%	62.9%
After	37.1%	33.5%	37.1%

Table 7.1. Percentage of ions that are ionized before ('Before') and after ('After') the reflection at the second barrier.

For the returning ions the ionization distribution is nearly flat for all three configurations, implying that for these ions the strength of the magnetic field seems not to have an enhancing effect on ionization.

To compare which fraction of the ions did get ionized before and after the reflection, the probabilities have been added. The results are presented in Table 7.1 for the three different configurations at electron beam energies of  $E_e = 10 - 11 \text{ keV}$ ,  $E_e = 12 - 13 \text{ keV}$  and  $E_e = 13 - 14 \text{ keV}$ . The probability to be ionized before the reflection is larger than 60% in all cases. The '6T-6T'-configuration has a slightly higher ionization probability before the reflection indicating that the ionization occurs earlier than in the case where a low field region is used. This can be explained by the fact that if an ion is injected with initial conditions that allow for ionization, the higher current density will lead to faster ionizations.

### 7.2.3 Magnetic field at first ionization

Figure 7.4 shows histograms presenting the probability for an injected ion to undergo the first ionization at a certain magnetic field strength. It can be seen that both configurations

with a low-field region have a large fraction of the ionization happening at  $B = 1 - 1.5$  T. Including ionizations that occur in the very low field just after the collector, most of the first ionizations happen at a low magnetic field where the electron beam has a larger radius. However, it can also be observed that the percentage to undergo the first ionization in the high magnetic field is not negligible. Especially, in the case of the '1T-6T'-configuration this means that there are ions that pass the low-field region without ionization. Only after reaching the high-field region, they obtain conditions that allow them to be ionized. The histogram of the '6T-6T'-configuration shows as expected a peak at where the magnetic field reaches its maximum. However, it can also be observed that many ionizations occur in low-field regions. This has to be taken into account when defining the size of the potential well for this configuration, since otherwise a considerable fraction of ions can be lost.

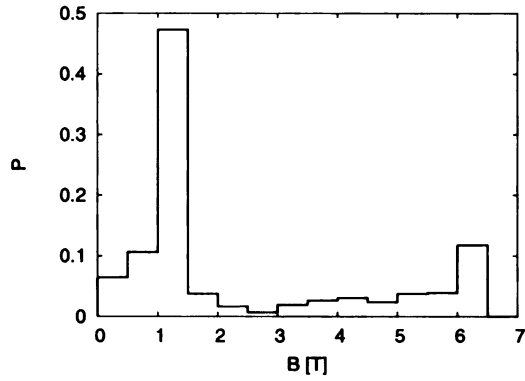
#### **7.2.4 Charge state after successful capture**

It is interesting to look at the charge state when the ion has turned around for the second time, i.e., considered to be captured. Figure 7.5 shows histograms of the charge states at this point. It can be observed that for both configurations including a low-field region about 50% of the ions were ionized just once. For higher charge states the percentage continuously decreases for an ion to end up in this charge state. The highest charge state observed is the  $6^+$ -state. For the '6T-6T'-configuration the percentage is increased for an ion to be captured with a higher charge state. Charge states up to  $10^+$  are observed after just one round-trip.

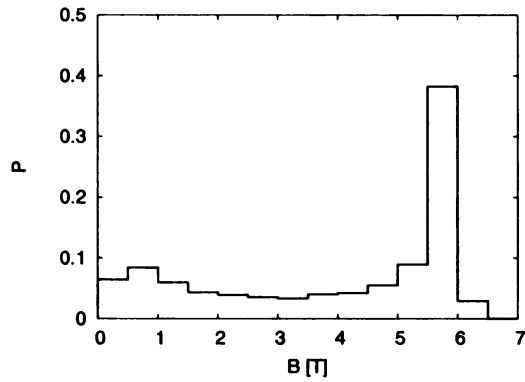
The results imply that for ions that are captured charge breeding is faster if a configuration is used that only includes a high-field region.

#### **7.2.5 Comparison between the '1T-6T' and the '6T-1T' configuration**

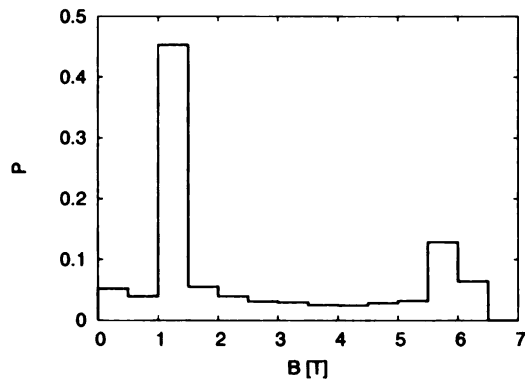
A surprising fact is the significantly lower acceptance of the '6T-1T'-configuration, even though it has a similar magnetic field distribution as the '1T-6T'-configuration. This means



(a)

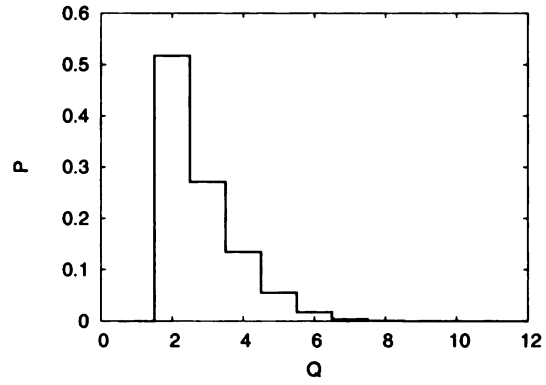


(b)

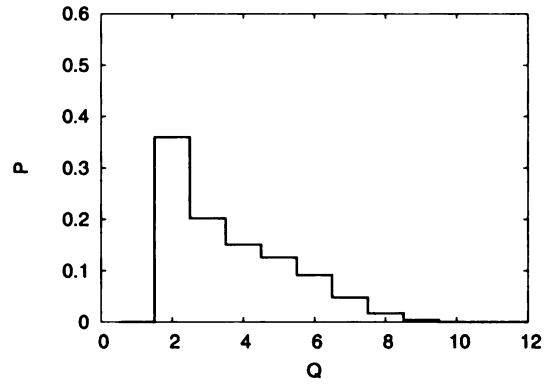


(c)

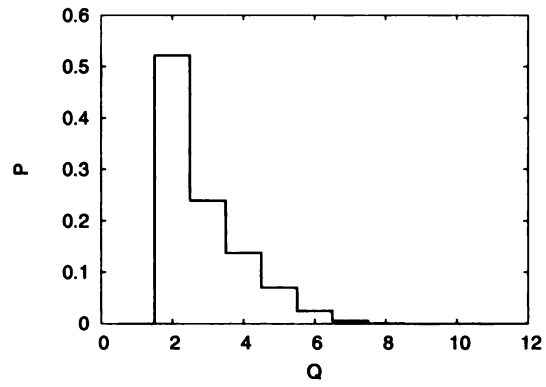
Figure 7.4. Histogram of the probability for an ion to undergo the first ionization at a certain magnetic field. The histograms show the three different cases (a): '1T-6T', (b): '6T-6T', (c): '6T-1T'. The electron beam energy in the trap is  $E_e = 12 - 13$  keV.



(a)



(b)



(c)

Figure 7.5. Histogram of the charge state of the ion, when it is considered captured. The histograms show the three different cases (a): '1T-6T', (b): '6T-6T', (c): '6T-1T'. The electron beam energy in the trap is  $E_e = 12 - 13$  keV.

that the presence of a high or low magnetic field alone cannot be the single determining factor for the efficiency of a configuration. The sequence in which the ion experiences the different fields seems to have an important role in determining the capture probability. One hint why the ‘6T-1T’-configuration offers relatively poor acceptance can be obtained by looking at the fate of the ion after being injected.

Table 7.2 shows the percentage of different processes that can happen after an ion is injected in the trap as discussed in Section 5.1. For both the ‘1T-6T’ and ‘6T-6T’ configurations the dominant ion loss mechanism is when an ion returns to the injection point without having been captured. Other processes leading to ion losses only accumulate to a few percent, so that about 12-13% of the injected ions are captured.

Comparing these numbers to those for the ‘6T-1T’-configuration, it can be observed that the ion loss mechanism of hitting the wall has gained importance. About 17% of all ions hit the electrode wall and about 74% of the ions are lost by not being ionized during the round-trip. This implies that the ‘6T-1T’-configuration seems to offer a less effective radial confinement of the ions, thus leading to more ions hitting the wall.

### 7.3 Electron beam energy

Figure 7.6 shows the capture probability as a function of emittance for different electron beam energies. For each of the three magnetic field configurations three different electron beam energy ranges have been used. As expected, the capture probability increases with decreasing electron beam energy. As noted in Section 6.2, the Lotz cross-sections are highest for electron beam energies that are about 1.5 times larger than the ionization potential of the least bound electron. Since for the first electron removals the ionization potential is quite low, higher cross sections are expected for lower electron beam energies in the trap. However, since electron energies of about 10 keV are relatively high compared to the energy needed to remove the second electron from an iron ion ( $I = 16.2$  eV), the increase

	'1T-6T'	'6T-6T'	'6T-1T'
$(E_e = 10 - 11 \text{ keV})$			
Trapped	14.72%	12.60%	9.41%
Wall	0%	2.25%	16.80%
Lost	85.27%	85.13%	73.61%
Reflected	0%	0.02%	0.17%
$(E_e = 12 - 13 \text{ keV})$			
Trapped	13.84%	11.89%	8.91%
Wall	0.01%	1.91%	16.58%
Lost	86.14%	86.17%	74.33%
Reflected	0%	.02%	0.18%
$(E_e = 13 - 14 \text{ keV})$			
Trapped	13.68%	11.75%	8.77%
Wall	0.01%	1.90%	15.72%
Lost	86.30%	86.33%	75.32%
Reflected	0%	0.02%	0.18%

Table 7.2. Percentages for capture and various loss mechanisms. *Trapped* refers to the case, when an ion is considered captured. *Wall* refers to the case, when an ion is lost by hitting an electrode. *Lost* refers to the case, when an ion is not trapped after one round-trip. *Reflected* refers to the case, when an ion is reflected by the first potential barrier.

in capture probability is rather small. This means that the capture probability is not significantly reduced if higher electron beam energies, as needed for breeding to higher charge states, are used in the trap.

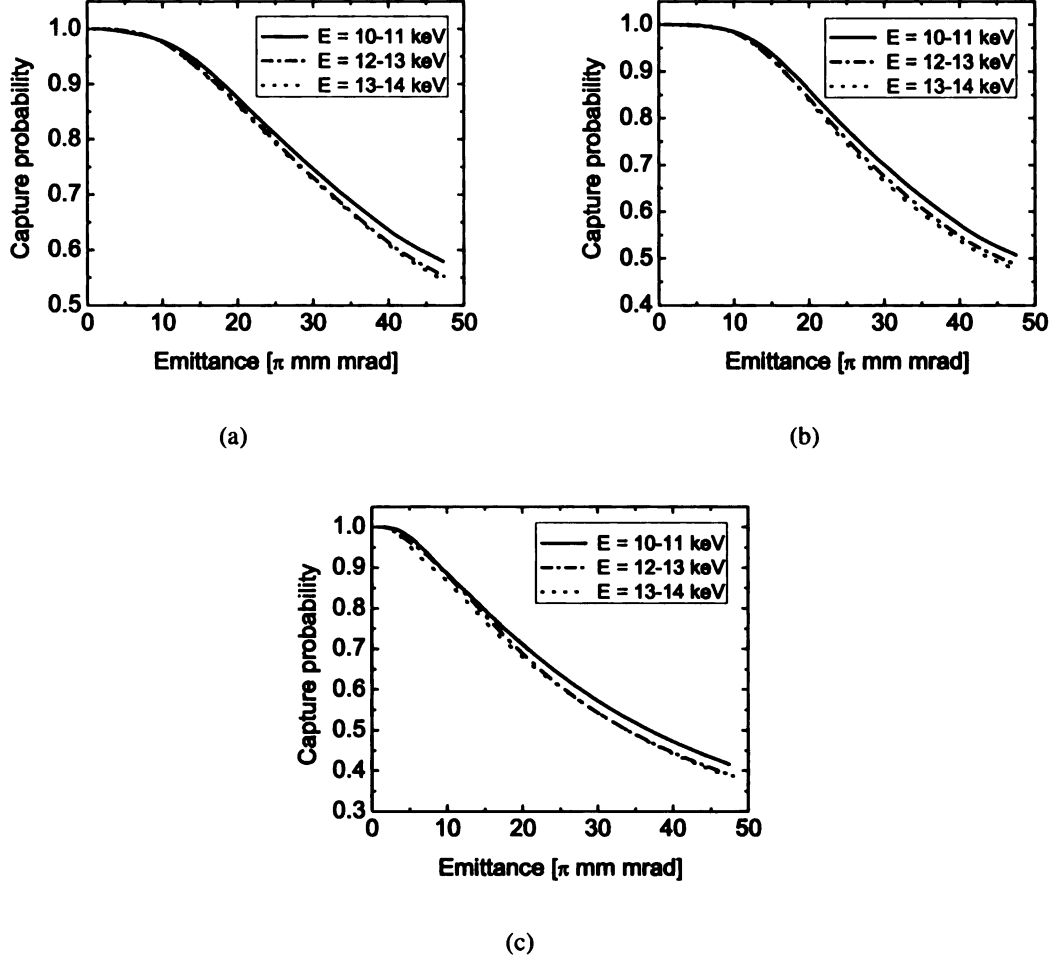


Figure 7.6. Comparison of the capture probability as a function of emittance for different electron beam energies. Three different configurations are considered with (a): '1T-6T', (b): '6T-6T' and (c): '6T-1T'. The electron current is  $I_e = 2.5$  A.

## 7.4 Electron beam current

Figure 7.7 shows the capture probability as a function of emittance for three different electron beam currents from  $I_e = 0.5$  A to  $I_e = 2.5$  A. All calculations were performed for the ‘1T-6T’-configuration at an electron beam energy of  $E_e = 12 - 13$  keV in the trap. The figure shows that the capture probability increases with larger electron beam currents. Even for small emittance an electron current of around  $I_e = 1.5$  A is needed to obtain a capture probability close to unity.

Table 7.3 shows the percentage of ionizations that occurred before the reflection at the second potential barrier, and after it. For the lower current (0.5 A) the number of ions being ionized before or after the reflection is about the same. This indicates that the  $1^+ \rightarrow 2^+$  ionization slows down which is highly undesirable for the capturing of ions. One solution could be a longer trapping region, so that the ions spend more time inside the electron beam.

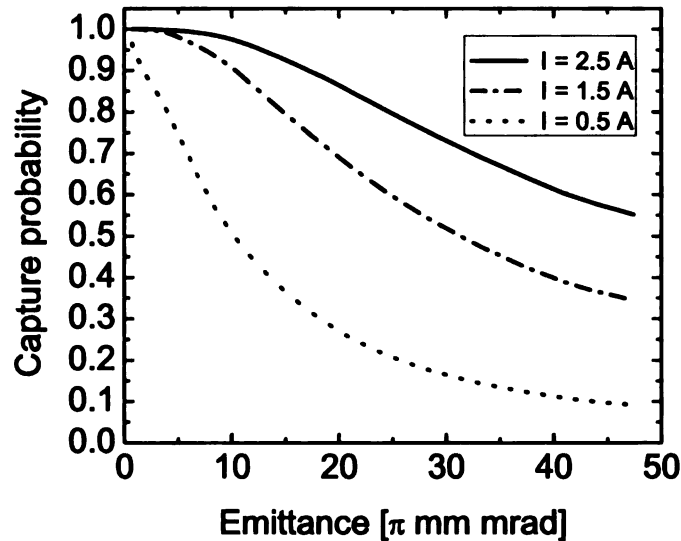


Figure 7.7. Comparison of the capture probability as a function of emittance for different electron beam currents for the ‘1T-6T’-configuration. The electron beam energy inside the trap is  $E_e = 12 - 13$  keV.

	$I_e = 0.5 \text{ A}$	$I_e = 1.5 \text{ A}$	$I_e = 2.5 \text{ A}$
Before	56.4%	60.4%	62.8%
After	43.6%	39.6%	37.2%

Table 7.3. Percentage of ions that are ionized before ('Before') and after ('After') the reflection at the second barrier for three electron beam currents with an electron beam energy of  $E_e = 12 - 13 \text{ keV}$ .

## 7.5 Trap dimensions

Figure 7.8 shows the capture probability as a function of emittance for the '1T-6T' and '6T-6T' configurations for different dimensions of the trap. In one case trap lengths are used as specified in Section 6.1, and in the other case the length of a field section is increased by 20 cm. For the '1T-6T'-configuration the low-field region is made 20 cm longer, whereas for the '6T-6T'-configuration the length of the high-field region is increased. As expected, the capture probability is increased if the trap is made longer. The capture probability of the extended '6T-6T'-configuration is higher for small emittance values as compared to the extended '1T-6T'-configuration. However, for emittance values larger than  $\epsilon = 15 \pi \cdot \text{mm} \cdot \text{mrad}$  the extended '1T-6T'-configuration offers a higher capture probability. It can be observed that for emittance values higher than  $\epsilon = 15 \pi \cdot \text{mm} \cdot \text{mrad}$  the difference between the '1T-6T' and the '6T-6T' configurations is somewhat larger for the setup with the longer trapping region.

The results imply that by making the trapping region longer, the overall capture probability does improve as expected. For low emittance values an extended high magnetic field region seems to benefit capturing most, however for large ion beam emittance the necessity for a low-field region is apparent.

Table 7.4 shows the percentage of ionizations occurring before and after the reflection at the second potential barrier. As expected the percentage of ions that are ionized before reflection is increased, however still a large percentage of ions undergoes ionization only

	'1T-6T'	'1T-6T' long	'6T-6T'	'6T-6T' long
Before	62.8%	63.5%	66.1%	68.1%
After	43.6%	36.5%	33.9%	31.9%

Table 7.4. Percentage of ions that are ionized before ('Before') and after ('After') the reflection at the second barrier. 'Long' indicates that the trapping region was made 20 cm longer. The electron beam energy is  $E_e = 12 - 13$  keV.

during the second half of the round-trip. This implies that increasing the trapping region even further would be of benefit for ion capturing.

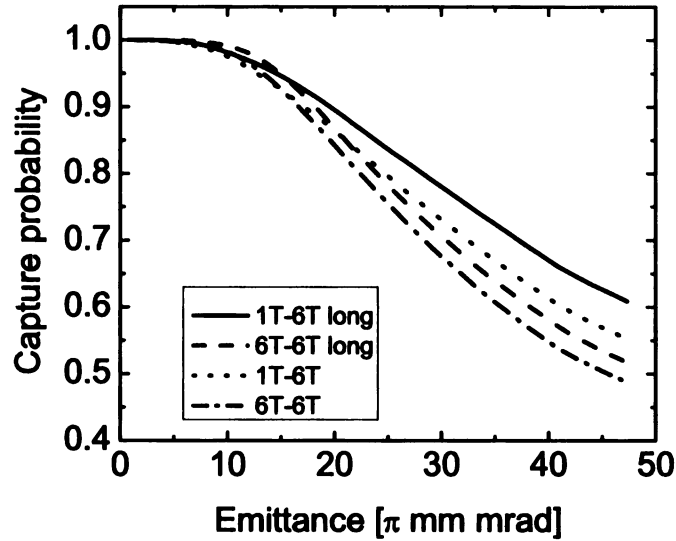


Figure 7.8. Comparison of the capture probability as a function of emittance for different trap lengths. 'Long' indicates that the trapping region was made 20 cm longer. The electron beam current is  $I_e = 2.5$  A and the electron beam energy is  $E_e = 12 - 13$  keV.

## 7.6 Initial axial energy

Figure 7.9 shows the capture probability as a function of emittance for different initial axial energies of the injected ions. The '1T-6T'-configuration is used together with an electron

beam energy of  $E_e = 12 - 13$  keV in the trap. Ion beam energies have been chosen such that the ions have energies of 0.8, 1.6, 2.4 keV when passing the first potential barrier on axis, including electron beam space charge effects.

It can be observed that changing the axial energy of the incoming ions does not greatly affect the capture probability. Obviously, this only holds true if the ions still have a considerable energy when passing the first potential barrier. There is a slight increase of the capture probability for a lower initial axial energy. Ions having a higher initial axial energy have consequently a lower capture probability. A remarkable feature for ions with a higher axial energy is that the capture probability at very low emittance values does not reach unity. The capture probability increases up to a maximum value for increasing emittances and then decreases again. The explanation is that for a lower emittance the ions stay near the electron beam axis. Thus the ion is moving close to the radial potential minimum. This, together with the higher initial axial energy, means that the ions obtain such a large axial velocity that some do not spend enough time in the trap to be ionized.

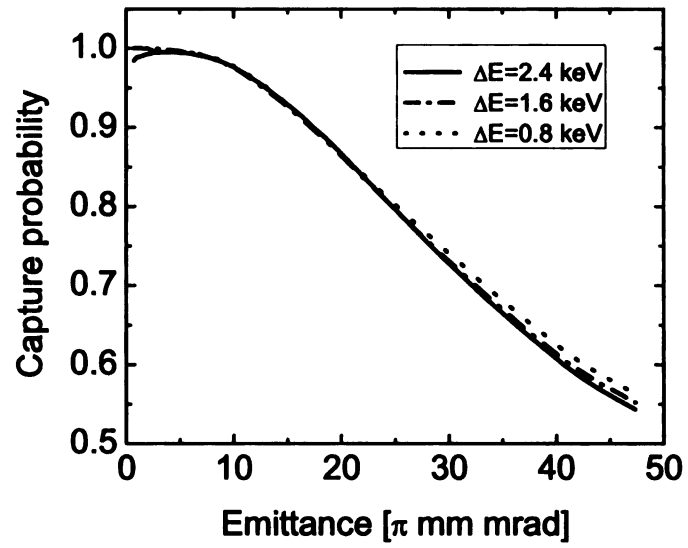


Figure 7.9. Comparison of the capture probability as a function of emittance for ions with different initial axial energies. The electron beam energy inside the trap is  $E_e = 12 - 13$  keV.

# Chapter 8

## Summary and conclusions

Simulations were performed to model the ion movement and charge evolution inside an EBIT. Acceptance calculations were performed for different trap configurations to obtain the capture probability. The following important results have been obtained:

- For low emittance values a trap configuration only including a high magnetic field has a higher capture probability than a configuration that has a low-field as well as a high-field region. For higher emittance the configuration including the low-field region offers higher capture probabilities, however only if the ions pass the low-field region first after injection. If the sequence of the regions is changed, the capture probability decreases drastically.
- By increasing the length of the trap, the capture probability is also increased. For longer traps the high-field-only configuration offers better results for low emittance values of the injected ion beam. However, it gives lower capture probabilities for higher emittance values, when compared to the configuration including a low-field region.
- A high-field-only configuration has the advantage that captured ions reach a higher charge state after one round-trip, so that the charge breeding speed is expected to be increased for such a configuration.

- The electron beam energy does not have large effects on the capture probability, if it is kept above 10 keV. Since this is the desirable value for charge breeding into highly charged states, no great changes are expected if the energy inside the trap is increased.
- The electron beam current has a very significant effect on the capture probability. Efforts should be made to obtain a high electron current since the efficiency of the continuous injection into the EBIT is highly dependent on this parameter.

The simulation results indicate that a trap configuration with a long low-field region and a shorter high-field region would be a viable solution, providing good capture efficiencies ( $>70\%$ ) for ion beam emittances of up to  $\epsilon = 37 \pi \cdot \text{mm} \cdot \text{mrad}$  at 9.6 keV.

Improvements can still be done to the simulation code, which may still change the results somewhat but not in a major fashion. The change of the electron beam energy to the space charge it creates could be implemented in a self-consistent way. This may lead to much longer simulation times but could be applied to a few test cases.

# **APPENDICES**

# Appendix A

## Function for the ionization process

The source code of the function is presented in which the Monte Carlo method is used to model the ionization. The virtual function 'TimeTest' is declared in the class where the equation of motions are solved with the Runge-Kutta algorithm. 'TimeTest' is defined in the class 'TEbitFast' which consists of basic simulation functions.

```
// tMC: time between two integration steps
// rad: radial coordinate of the ion
// z: axial position of ion
// kin: kinetic energy of ion
// vzz: axial energy of ion

bool TEbitFast::TimeTest(double tMC, double rad,
double z, double kin, double &vzz)
{
    bool ok;
    ok = true;
    // get electron beam radius
    Ebit.SetERad(z, ERad);
    // get axial magnetic field
    Ebit.SetMag(z, rad, B_z);
    // get total potential
    Ebit.SetPot(z, U_p);
    // get electrode radius
    Ebit.SetRad(z, r_tube);
    // get prefactor in front of space charge potential
    // and electron beam energy
    Ebit.SetUFac(z, Ufac, Eel);
```

```

// time spent in electron beam
tEB = tEB + tMC;
// total time
tTOT = tTOT + tMC;

// if ion is inside electron beam
if (rad<ERad)
{
    // get cross section
    CBXSDump.DumpXSec(xSec, Z, Q_e, Eel);
    // calculate t12
    t12 = ERad*ERad*M_PI*echarge/(xSec*Ie*.8);
    // random number
    rNR=Random.One();
    // probability for ionization
    p=1-exp(-tMC/t12);

    // if ionization occurs, charge is reduced by one
    if(rNR<p)
    {
        // add one incident
        N_ion[Q_e-1]++;
        // add 1
        Q_e=Q_e+1;
        // new q-m-proportion
        QOverM = (Q_e*Const.GetE())/(Mass_u*Const.GetU_kg());
        // new q-m-proportion in TEBit-class
        Ebit.SetQOverM( QOverM);
        // output at first ionization
        if(Q_e == 2)
        {
            histo << z << " " << vzz << " " <<
            rad << " " << B_z << " " << Eel << endl;
        }
    }
}
// if ion is outside the electron beam
else
{
    // time spent in electron beam is set to zero
    tEB=0.;
}

```

```

}
// if ion has turned
if(vzz*vz_old < 0.)
{
    // increase turning-counter by one
    par++;
    // if turn is after the first potential barrier
    if(par == 1 && z > z_step + toll)
        turn = 1;
    // ion had two turns
    if(par > 1)
    {
        // if ion did underto at least
        // one ionization it is trapped
        if(Q_e > 1)
            N_trapped++;
        trapcond << ratio << "\t" << vRad << "\t"
        << vPhi << " " << vzz << " " << vz_old << " "
        << z << " " << Q_e << endl; // output
        // abort simulation
        ok = false;
    }
}
// if ion reaches electrode tube
if(rad >= r_tube)
{
    // ion did not turn
    if(par == 0)
    {
        wall_c++;
        wallc << z << "\t" << rad << "\t"
        << vzz << "\t" << r_tube << endl;
    }
    // ion did turn, however is not lost yet
    if(par == 1 && z > -.545)
    {
        wall_c++;
        wallc << z << "\t" << rad << "\t"
        << vzz << "\t" << r_tube << endl;
    }
    ok = false; // abort simulation
}

```

```

}
if(ERad == 0.)
    pot = 0.;
// potential approximation at collector
if(ERad != 0 && potc == 0)
    // assuming that the space charge
    // potential on-axis is -513 keV
    // axial velocity is changed
    // for ions that are off-axis,
    // so that total energy is kept constant
    {
        vzz = sqrt(vzz*vzz - 2.*(pot+513.*Const.GetE())/
            (Mass_u*Const.GetU_kg()));
        potc = 1;
    }

// how many ions leave the system
if(loss_par == 0 && z < -.545 && par > 0)
{
    // if ion did pass the
    // potential barrier initially
    if(turn == 1)
    {
        loss_c++;
    }
    // if ion got reflected by
    // initial potential barrier
    else
    {
        if(Q_e == 1)
            refl_c++;
        else
            reflion_c++;
    }
    loss_par = 1;
}
// velocity from this integration-step
// will be the old velocity in the
// next integration-step
vz_old = vzz;

```

```
    return ok; // if false simulation is aborted  
}
```

## **Bibliography**

## Bibliography

- [1] D. J. Morrissey, B. M. Sherrill, M. Steiner, A. Stolz, I. Wiedenhoever, Nucl. Instr. and Meth. B **204**, 90 (2003)
- [2] D. J. Morrissey, B. M. Sherrill, in: *The Euroschool lectures on physics with exotic beams, Vol. 1* (2004)
- [3] G. Bollen, D. Davies, M. Facina, J. Huikari, E. Kwan, P. A. Lofy, D. J. Morrissey, A. Prinke, R. Ringle, J. Savory, et al., Phys. Rev. Letter **96**, 152501 (2006)
- [4] R. Ringle, T. Sun, G. Bollen, D. Davies, M. Facina, J. Huikari, E. Kwan, D. J. Morrissey, A. Prinke, J. Savory, P. Schury, S. Schwarz, C. S. Sumithrarachchi, Phys. Rev. C **75**, 055503 (2007)
- [5] P. Schury et al., Phys. Rev. C **75**, 055801 (2006)
- [6] S. Schwarz et al., Nucl. Instr. and Meth. B, in press
- [7] S. Schwarz et al., Rev. Sci. Instrum. **79**, 02A706 (2008)
- [8] T. Lamy, R. Geller, P. Sortais, T. Thuiller, Rev. Scient. Instr. **77** (2006) 03B101
- [9] T. Lamy, Rev. Scient. Instr. **77** (2002) 717
- [10] O. Kester et al., Nucl. Instr. and Meth. B **204**, 20 (2003)
- [11] F. Wenander et al., Rev. Sci. Instrum. **77**, 03B104 (2006)
- [12] A. Pikin, J.G. Alessi, E.N. Beebe, A. Kponou, K. Prelec, Rev. Sci. Instrum. **77**, 03A109 (2006)
- [13] R.E. Marrs, D.R. Slaughter, AIP Conf. Proc. **475**, 322 (2006)
- [14] R.E. Marrs, M.A. Levine, D.A. Knapp, J.R. Henderson, Phys. Rev. Lett. **60**, 1715 (1988)
- [15] M. Froese, C. Champagne, J.R. Crespo Lopez-Urrutia, S. Epp, G. Gwinner, A. Lapierre, J. Pfister, G. Sikler, J. Ullrich, J. Dilling, Hyperfine Interactions **173**, 85 (2006)

- [16] P. Delheij, L. Blomeley, M. Froese, G. Gwinner, V. Ryjkov, M. Smith, J. Dilling, *Hyperfine Interactions* **173**, 123 (2006)
- [17] F. Currell and G. Fussmann, *IEEE Trans. Plasma Sci.* **33**, 1763 (2005)
- [18] E. D. Donets and V. P. Ovsyannikov, *Sov. Phys. JETP* **53**, 466 (1981)
- [19] R. W. Schmieder, C. L. Bisson, S. Hanley, N. Toly, A. R. Van Hook, J. Weeks **61**, 259 (1990)
- [20] M. A. Levine, R. E. Marrs, J. R. Henderson, D. A. Knapp, M. B. Schneider, *Phys. Scr.* **22**, 157 (1988)
- [21] G. Herrmann, *Journal of Applied Physics* **29**, 127 (1958)
- [22] L. Brillouin, *Physical Review* **67**, 260 (1945)
- [23] G. Fussmann, C. Biedermann, R. Radke, *NATO ASI Series*, 1998
- [24] J. Gillaspay, *Trapping Highly Charged Ions: Fundamentals and Applications*, Nova Science Publishers, Inc, (2001)
- [25] W. Lotz, *Z. Phys.* **206**, 205 (1967)
- [26] F. Wenander et al., *REXEBIS* (1999)  
<http://doc.cern.ch/archive/electronic/cern/preprints/open/open-2000-320.pdf>
- [27] T. Schenkel, A. Persaud, A. Kraemer, J. W. McDonald, J. P. Holder, A. V. Hamza, D. H. Schneider, *Rev. Sci. Instrum.* **73**, 663 (2002)
- [28] S. Humphries Jr., *Charged particle beams*, John Wiley & Sons Inc, (1990)
- [29] X. Wu, M. Doleans, Q. Zhao, G. Gorelov, T.L. Grimm, F. Marti, R.C. York, D. Lawton, G. Bollen, in: *Proc. Particle Accelerator Conference 2007, Joint Acc. Conf. Website*
- [30] W. H. Press et al., *Numerical Recipes 3rd Edition*, Cambridge University Press, (2007)
- [31] M. W. Garrett, *J. Appl. Phys.* **22**, 9 (1951)
- [32] W. Lotz, *J. Opt. Soc. Am.* **57**, 873 (1966)
- [33] W. Lotz, *J. Opt. Soc. Am.* **58**, 236 (1967)
- [34] W. Lotz, *J. Opt. Soc. Am.* **58**, 915 (1967)
- [35] W. Lotz, *Z. Phys.* **216**, 241 (1968)
- [36] C. Guenaut et al, *Hyperfine Interactions*, **173**, 113 (2006)

MICHIGAN STATE UNIVERSITY LIBRARIES



3 1293 02956 8536